Defects in Pentacene Thin Films Grown by Supersonic Molecular Beam Deposition

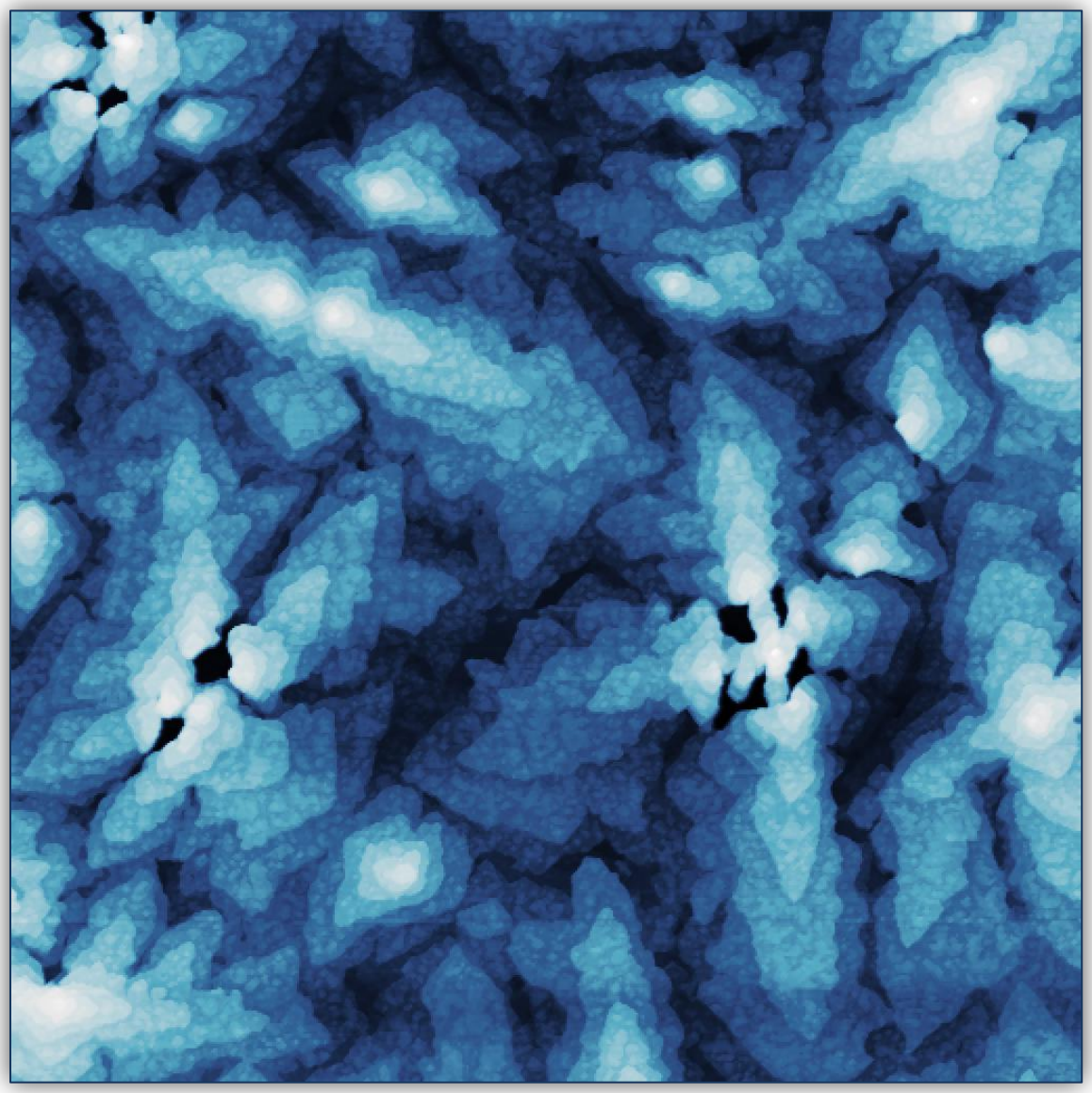

Bart Wit

University of Groningen
Zernike Institute for Advanced Materials

University of Groningen
Zernike Institute for Advanced Materials
Surfaces and Thin Films

Defects in Pentacene Thin Films Grown by Supersonic Molecular Beam Deposition

Bart Wit
S1615831

Supervisor
Prof. Dr. Petra Rudolf

Pentacene is a very promising organic semiconductor for applications in thin film devices. However, to achieve a good device performance, it is very important to grow thin films with the least amount of defects and grain boundaries as possible. One of the ways to improve the film quality is to use the novel deposition technique Supersonic Molecular Beam Deposition. In this work, the defect structures in pentacene films grown with this technique and those grown with the conventional technique of Organic Molecular Beam Deposition are compared. This was attempted by partial etching of the sample to reveal dislocations. Even though the etching method did not perform properly, it was found that the same defects are likely to be present. The main analysis technique was contact mode Atomic Force Microscopy. With this technique evidence for defects was found, as well as some other interesting characteristics.

Table of contents

Introduction

Organic molecules have always been important in science and development because of the inexhaustible amount of possible molecular structures with just as many possible applications. However, it was not until the 1950's that organic semiconductors were discovered. Nowadays, a broad range of organic materials which are able to conduct electricity are known. All of these materials, both small molecules and polymers, feature a conjugated π-system. Within this system, the orbitals of the electrons delocalize throughout the molecule. Organic semiconductors have long been recognized as potentially useful materials in electronic devices. This is because organic semiconductors offer some significant benefits over their inorganic counterparts which are commonly used nowadays. First of all, the costs associated with using inorganic materials are generally very high compared to those associated with organic semiconductors. The reason for the relative high cost of the inorganic semiconductors is twofold. On one hand, it is difficult to make highly pure and defect free single crystals of silicon, which is the basic material used in every electronic application. Even the most efficient process used to make these single crystals requires large amounts of energy and is therefore very expensive. Since this process is almost completely optimized by now, no significant improvement is to be expected in this area. Also, many of the other inorganic materials used in applications consist of rare metals, either in pure form or in compounds. Since these materials are quite rare, they are also very expensive. This will probably get worse in the future, when these materials become even scarcer.

With organic materials, these drawbacks are mostly absent. These compounds consist mainly of carbon and hydrogen which are abundant. Also, it is possible to make films suitable for device applications with easy and cost efficient techniques like drop casting or spin coating. The monetary argument is not the only one in favour of organic semiconductors. Also, some physical properties of these materials are much better. First of all, they are much lighter, which is obviously an advantage in applications such as cell phones. Also, many of these materials, most notably the conducting polymers, are much more flexible than silicon single crystals. This can be exploited in bendable displays and other applications. Another advantage is the tunability of organic molecules. It is relatively simple to modify the properties of the molecules to fit a certain application. Using chemical synthetic methods, the structure of the molecule can be altered to improve solubility, change the band gap of the material and so forth. Despite these advantages, making commercially viable devices with organic semiconductors is still quite a challenge. This is because, until now, the benefits of using these materials are usually not sufficient to outweigh the drawbacks. The major drawbacks are the limited performance and stability of the organic electronic devices. The limited performance stems from the fact that these materials consist of individual molecules. These molecules interact only via weak Van de Waals forces and sometimes trough π-π stacking. This means that there is little orbital overlap between the molecules. Therefore, conduction can only take place if the molecules are aligned properly. This requires highly crystalline thin films. The stability issue is mainly caused by the sensitivity of thin films of organics to oxygen and water. Through extensive research, these drawbacks have been decreased significantly. By tuning the molecules, compounds with higher stability and better conducting properties have been found. Also, the quality of the thin films has been improved, significantly increasing device performances. Due to these efforts, several commercially viable applications have already been realized. For examples Organic Light Emitting Diodes (OLEDs) are used in mobile phone displays and televisions.

In this work, the results of an investigation on defect structures in pentacene thin films grown on silicon oxide will be presented. These films have been deposited using both the conventional technique Organic Molecular Beam Deposition (OMBD) and the novel technique Supersonic Molecular Beam Deposition (SuMBD). In this work, the focus will be on line dislocations in the second monolayer (ML) of the pentacene thin films. This is because these defects can easily be made visible by Atomic Force Microscopy (AFM) after a short etching step using sulphuric acid.

Expanding the knowledge about these defect structures is relevant for two reasons. First of all, pentacene is a very promising material for application in organic electronic devices such as Thin Film Transistors (TFT). However, so far, the inability to make layers of sufficient quality is a real problem. Defects in the first few monolayers reduce the device performance significantly. Therefore, a better understanding of the defect structures could help improve device performances. On the other hand, understanding the differences and similarities between the defect structures in the films grown with both techniques, OMBD and SuMBD, could give more insights in to the latter. Since the SuMBD technique is quite new, not everything is completely understood about it. Therefore, any details of the performance of SuMBD with respect to OMBD are useful to improve the knowledge about SuMBD.

In the first chapter of this thesis, the theoretical background of this work will be outlined. The first part of the theory will cover organic semiconductors in general and pentacene in particular. Also, the thin film devices based upon these materials will be described. Subsequently, the theory behind thin film growth and the growth techniques SuMBD and OMBD will be discussed. The last part of the theory section will be devoted to the analysis methods used to characterize the deposition and the resulting thin films. This includes AFM, the quartz microbalance, Time of Flight measurements and film etching. The next chapter will cover the experimental setup for the various techniques used. Also, the methods used for cleaning and etching the samples will be given. Special attention will be devoted to the SuMBD setup as it is the main technique. In the third chapter, the results obtained in this work will be presented and discussed. This will include the results of the etching experiments as well as other interesting observations. Finally, a conclusion and an outlook will be given.

Theory

In this chapter, the theoretical foundation for the rest of this work will be outlined. First, a section is devoted to the organic semiconductors. This will also cover pentacene in particular. In the second section, the theory behind thin film devices such as the aforementioned Thin Film Transistors (TFTs) will be discussed. After this, thin film growth will be covered. This is followed by the theory behind the two growth techniques used, Organic Molecular Beam Deposition (OMBD) and Supersonic Molecular Beam Deposition (SuMBD). Also, the advantages and disadvantages of both techniques are compared on a theoretical basis. The next sections deal with analysis methods. This encompasses the theory behind the analysis method of choice, Atomic Force Microscopy (AFM), and in particular the Lateral Force Microscopy (LFM) and Transverse Shear Microscopy (TSM) modes. Also, the theory behind time of flight and quartz microbalance measurements will be covered briefly as these were used during film growth. The last section is about the theory behind the etching technique used to investigate the defects in the pentacene thin films.

Organic semiconductors

Since the discovery of the semiconducting properties of polyacetylene in the 1950's, a broad set of organic semiconductors has been found. Some of these are also polymers, such as polyphenylenes, polyfluorenes, polypyrroles and polythiophenes. Other organic semiconductors are oligomers or smaller molecules, such as acenes, thiophenes, phthalocyanines and fullerenes. These families do not only include the native compounds but also many derivatives. The common theme among these compounds is the existence of a conjugated π-orbital structure. The polymer backbone or the molecular framework consists of sp^2 hybridized carbon atoms. The remaining p-orbitals overlap to from large delocalized orbitals. This electron delocalization is one of the major factors in determining the conductivity of the materials. The overlap of these π-orbitals of different molecules is also very important, especially so in the case of small molecules.

As mentioned, for each of the molecular families of semiconductors, many derivatives have been synthesized. These derivatives were engineered to have different properties, such as a different band gap or better solubility. In the case of polymers, the band gap can be tuned by choosing different monomers in so-called donor-acceptor alternating co-polymers.[1] Also, the solubility is often enhanced by adding long alkyl chains to the monomers. In general, this makes processing these materials significantly easier while keeping the desired functionality nearly intact. In the case of molecules, many different functional groups can be used to improve solubility. However, these functional groups usually alter the crystal packing. This can be detrimental or beneficial to the properties of the film. An alternative approach to improve processing conditions is to synthesize precursor molecules, which can be converted into the desired molecule after the deposition of the film. Also, many different variations on the molecule can be made to tune the band gap.[2] Another important property of these materials that can be changed by chemical modification is the charge carrier type. Most of the aforementioned molecules are p-type conductors. This means that the charge carriers are predominantly holes. One notable exception is C_{60}, which is naturally an n-type semiconductor. That is, the electrons are the major charge carriers in this material. However, by adding electron withdrawing side groups, such as halogens, the materials can be modified such that they become n-type semiconductors. This demonstrates the power of the tunability of the organic semiconductors.[2]

One of the most promising organic semiconductors for applications is pentacene, $C_{22}H_{14}$. The structure of this molecule is shown in Figure 1 A. It can be seen that it consists of five fused aromatic rings. This is indeed a conjugated π-orbital structure. Due to the nature of the aromatic bonds, the molecule is completely flat. The length of the molecule is approximately 1.45 nm along the long axis. The bulk crystal structure of this material is triclinic with two molecules in the unit cell. These molecules are arranged in a herringbone configuration.[3] A top view of the pentacene crystal, with the herringbone structure, is shown in Figure 1 B. The interplanar spacing in a crystal is about 1.44 nm.

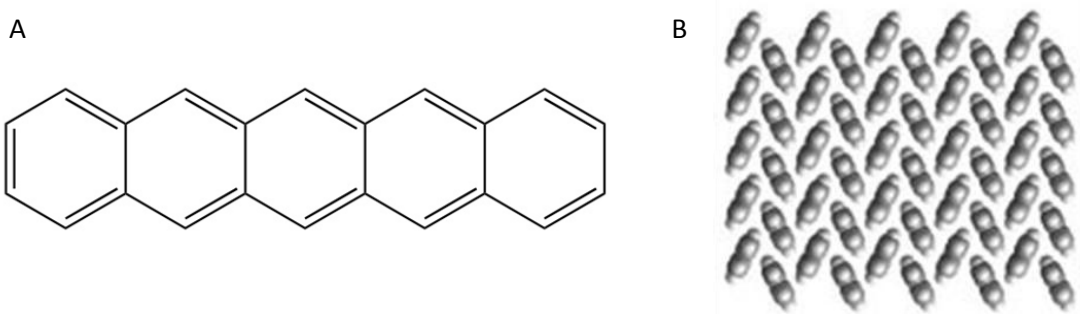

Figure 1: The structure of a pentacene molecule in a wireframe representation (A) and a top view of the pentacene crystal showing the characteristic herringbone structure (B).

However, in thin films a slightly distorted structure is more common, usually referred to as the thin film phase. The crystal symmetry is orthorhombic and the interplanar spacing is about 1.54 nm in this case.[4] Both phases can coexist in the thin film. The existence of the phases is dependent on the surface, the temperature and the film thickness, among other things.[5] In any case, the thickness of one monolayer is approximately 1.5 nm. A peculiarity recently discovered is that the first layer grows differently due to the interactions with the substrate. This causes the molecules in the first ML to stand upright without a tilt as in subsequent layers.[4] The second layer grows preferably with a 76° twist due to the differences in crystal packing.[6]

Thin film devices

One possible field of applications for organic semiconductors such as pentacene is that of the thin film devices. Even though these thin film devices are not investigated explicitly in this work, it is good to have a basic understanding of their function. This is because these applications pose certain requirements on the materials used. Knowing these requirements is essential when trying to engineer the materials for future application. A good example of a thin film device is the Thin Film Transistor (TFT). A schematic representation of a typical thin film transistor can be found in Figure 2. There are three electrodes, two gold electrodes on top and a bottom electrode which is the silicon substrate. The gate electrode and the active material are separated by a dielectric layer, in this case SiO_2. The current flow is between the source and the drain, trough the active layer. Here, the active layer is the organic semiconductor. The current flow can be controlled by changing the voltage on the gate electrode, while keeping the voltage between the source and the drain constant. A voltage applied to the gate can either switch the current on or off, depending on the type of semiconductor. The device shown is a top electrode configuration. however, the arrangements of the electrode and the materials used might vary between different devices. The basic function remains the same.

A number of parameters are important for a good device. First off all, the ratio between the on and off current should be sufficiently high. The higher this value, the easier the signal can be distinguished from random noise. Also, the threshold voltage, the applied gate voltage where the device switches on and off, is important. Usually, a value close to zero is preferred for applications.

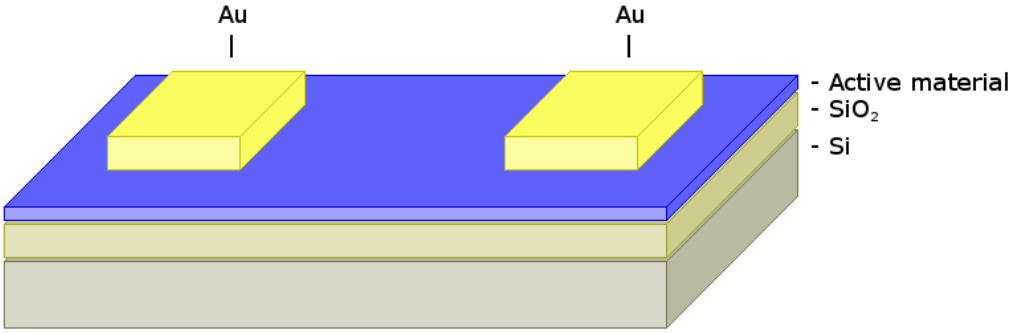

Figure 2: A schematic representation of a TFT

However, the most important parameter is the charge carrier mobility. Mobilities measured in field effect transistors are often referred to as field effect mobilities. They can be measured either in the linear or in the saturation regime of the device. This is a measure for the ease with which the holes or electrons move through the material. The higher the mobility, the faster the device can be switched. For state of the art devices, a sufficiently high mobility should be achieved. Besides the material itself, the quality of the active layer is important. Often, defects can act as trapping sites for the charge carriers, naturally decreasing their mobility. Especially the first few layers of material are important in organic semiconductors, as the larger part of the conduction goes through these layers. Also, a higher film quality, and thus less trapping sites, reduces hysteresis in the current flow. This shows that the ability to make highly crystalline thin films is crucial to the development of thin film devices based upon organic semiconductors. Several ways are being explored to improve the thin film quality. One of the most important ways is the application of a self assembled monolayer between the substrate and the organic semiconductor. In this work, a different approach is chosen. A novel technique, SuMBD, can be used to deposit organic molecules with significantly improved film quality.

A significant amount of research has gone towards measuring and optimizing the charge carrier mobilities in pentacene and other organic semiconductors. For amorphous and polycrystalline samples, the mobilities usually do not exceed 1 $cm^2V^{-1}s^{-1}$. However, some reports have shown mobilities in the order of 10 $cm^2V^{-1}s^{-1}$ in thin films of phthalocyanines. For single crystals of organics, measured mobilities can be as high as 40 $cm^2V^{-1}s^{-1}$.[1] The difference between the performance of single crystals and polycrystalline materials can be explained by the difference in transport mechanisms. In single crystals band-like transport dominates, while in samples with more defects that can act as trapping sites, this is not possible. Instead, conductivity is best explained by a thermally activated hopping mechanism.[7] In very high quality thin films, near band like transport can be achieved. However, In general, the measured mobilities are not comparable to those of inorganic materials. For example, the most important semiconductor, silicon, features mobilities that can be as high as 1400 $cm^2V^{-1}s^{-1}$ for electrons. In graphene, they can even be a factor ten or hundred higher.

The first pentacene TFT was reported in 1992.[8] The mobility measured in this device was $2 \cdot 10^{-3}$ $cm^2V^{-1}s^{-1}$. Much work and many reports on improved mobilities in pentacene TFTs have followed, where the most notable ones are the following: In 1997, a significantly increased mobility was achieved by functionalizing the SiO_x substrate with a self assembled monolayer of octadecyltrichlorosilane to achieve a mobility of about 1.5 $cm^2V^{-1}s^{-1}$.[9] Recently, in 2010, self assembled monolayers of phosphonates were used to achieve a maximum mobility of 4.7 $cm^2V^{-1}s^{-1}$.[10] Another route employed, using a polymeric dielectric as a gate material, yielded a hole mobility of 3.0 $cm^2V^{-1}s^{-1}$ in 2002[11] and of about 5.5 $cm^2V^{-1}s^{-1}$ in 2006[12]. Finally, the highest reported mobility of a pentacene layer grown on bare SiO_x using SuMBD deserves to be mentioned. This is 1.0 $cm^2V^{-1}s^{-1}$ and was reported in 2006. The method used, SuMBD, is the major growth technique used here.[13]

Thin film growth

As discussed earlier, the quality of a thin film can greatly affect the performance of a corresponding thin film device. This is because defects in the layers, such as grain boundaries, can greatly influence the mobility of the charge carriers in these layers. One of the important parameters for creating a good device is therefore the deposition method. There are many ways to make a thin film of an organic material. Examples are drop casting, spin coating, the Langmuir-Blodgett (LB) method, self assembly, Chemical Vapour Deposition (CVD) and Molecular Beam Deposition (MBD). Each of these methods offers different advantages and disadvantages. Also, not every method works equally well with the desired material. In this work, MBD is used exclusively, thus this will be covered in more detail. In particular, two variants of MBD were used. The first was Organic MBD, hereafter referred to as OMBD. This is a conventional technique for the growth of thin layers of an organic material. The second technique used was Supersonic MBD, or SuMBD. This is a novel technique. Both techniques rely on a molecular beam to transport material trough a vacuum from a source to the substrate. This material will be deposited on the substrate and a film will then grow under the right conditions.

The principle difference between OMBD and SuMBD lays in the way the molecular beam is generated and the properties of the beam itself. The techniques will be discussed in detail in the next section. Also note that these techniques are often referred to as OMBE and SuMBE, where the E stands for Epitaxy. However, this is more suitable in the case of epitaxial growth of the organic film, which is not applicable to this work.

Before reviewing both techniques in more detail, it is useful discuss a few aspects of MBD based thin film growth in general. That is, the general case of molecules arriving at the substrate from a material stream in a high vacuum. The arriving molecules can interact in various ways with the substrate. This is illustrated well with the schematic potential energy diagram shown in Figure 3. In the simplest case, the molecule can be reflected back into the vacuum. In Figure 3 this is shown for a molecule with high energy which cannot be dissipated. However, there are other possibilities such as a molecule arriving with very low energy that is reflected by a barrier to the first minimum. As the molecules never arrive on the surface, this does not contribute to film formation on the substrate. However, under the right circumstances, the molecule might stick to the surface. The probability that this happens is referred to as the sticking probability. Clearly, a non-zero sticking coefficient is required for film growth. If the molecule sticks on the surface, it is adsorbed. In general, molecules can adsorb in various ways. If there is only a weak Van der Waals interaction between the surface and the molecule, it is said to be physisorbed. If, on the other hand, the molecule interacts more strongly with the surface, for example trough a covalent bond, it is said to be chemisorbed. In general, there might be many different minima associated with physisorbed and chemisorbed states. Also, a third category of minima could be present. These are usually significantly deeper than those representing chemisoption. These minima are associated to chemical processes, such as dissociation or other chemical transformations. This is important in, for example, catalysis. If a molecule acquires sufficient energy, for example from a phonon, it can overcome the energy barrier between different states. In fact, it is rare that molecules have sufficient energy to go directly to a chemisorbed state. It is also possible that the molecule overcomes the energy barrier between the bound state and the free state. In other words, the molecule could re-evaporate. This is detrimental to film growth. Re-evaporation rates increase with substrate temperature. The flux of molecules reaching the surface together with the sticking probability and the re-evaporation rate determine the film growth rate. In the case of pentacene on silicon oxide, only physisorption is relevant.

The potential energy diagram for the molecule surface distance does not describe 2D movement of molecules on the surface. The cartoon in Figure 4 gives a good overview of the various processes that are possible. In general, molecules motion on a surface is known as surface diffusion.

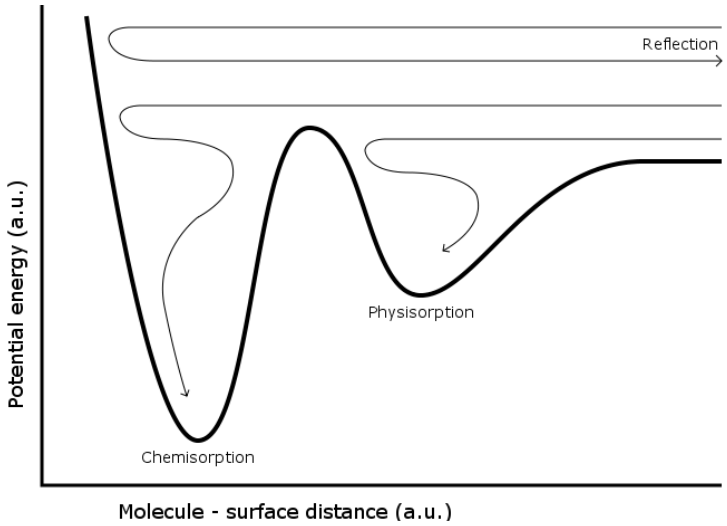

Figure 3: A simplified potential energy curve as a function of the molecule - surface distance. Three important possible interactions are represented by the curved arrows. These are physisorption, chemisorption and reflection.

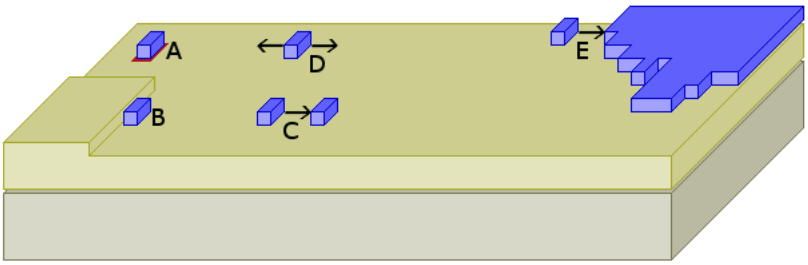

Figure 4: A cartoon representation of some important processes that take place on a surface during deposition. Molecules, represented by blue cubes, can adsorb at defect sites (A and B), nucleate new islands (C), diffuse across the surface (D) and attach to existing islands (E). The reverse of nucleation and island growth is also possible.

This is shown in Figure 4 D. Molecules diffusing on the surface interact with various other structures and molecules present on the surface. For example, they might encounter special sites on the surface to which they bind strongly. The molecules will get stuck at these sites for a certain period of time. Binding to special sites is shown in Figure 4 A and B for point defects and step edges. Also, they can meet other molecules and nucleate an island, as shown in Figure 4 C. Lastly, they can meet an existing island and attach to that. This is referred to as island growth and is shown in Figure 4 E. The reverse of these two processes is also possible. A nucleus might dissociate and molecules at the edge of an island could detach and continue diffusing over the surface. To describe these processes, the potential energy of the molecule as a function of its position on the surface should be considered. A useful analogy of island growth and surface diffusion is a normal gas – solid equilibrium. Only, this happens in 2D and additional interactions with the surface are possible.

When a molecule is adsorbed on a surface, it will sit at a position where the potential energy has a local minimum. Such a position is referred to as an adsorption site. On any given surface, there are many different adsorption sites. In between different adsorption sites, there will be a potential energy barrier. Diffusion can occur if the molecule has enough energy to overcome this potential energy barrier. In the case of a perfectly flat single crystal, the adsorption sites will all be identical with the same potential energy. However, for amorphous surfaces, there will be a more random distribution of sites with different potential energies. Defects on the surface, such as step edges and impurities, will introduce sites with a different potential energy which can be favourable or unfavourable compared to normal sites. The potential energy of a given site is also influenced by the occupancy of nearby sites. If the molecules interact attractively with one another, the potential energy for adjacent sites will be lower and vice versa. These potential energy differences will dictate whether island formation and growth are favourable. The activation barrier can also be different between different sites. For example, moving down a step edge can be accompanied by a lower or a higher barrier. In the latter case, the barrier is referred to as an Ehrlich-Schwoebel barrier. This barrier can trap molecules on the specific terrace or island they happen to be on.

For a more formal approach to surface diffusion, many factors have to be taken into account. However, a relatively simple method is to model the movement of the molecules as a series of thermally activated jumps. This is known as hopping. Surface diffusion is therefore adequately described by the molecular hopping rate Γ:

$$\Gamma = \nu \cdot P = \nu \cdot e^{\frac{-\Delta E}{kT}}$$

Here, P is the hopping probability, which is dependent on the activation energy ΔE, and ν is the attempt frequency. The attempt frequency is usually taken to be the vibration frequency of the molecule. This formula is valid for thermal equilibrium, where the internal energy of the molecule is equivalent to that of the surrounding. Otherwise and effective kT should be used. If the molecule has a higher internal energy, the hopping rate will be higher since its vibration frequency is higher Also, it is more likely that the molecule has the required energy to transverse the activation barrier.

The maximum distance a molecule can travel on the surface before desorbing is given by the diffusion length Λ:

$$\Lambda = \Gamma \cdot a \cdot \tau$$

Here, a is the lattice parameter and τ is the typical desorption time. A higher diffusion length is beneficial to film growth since the chance that a molecule meets another molecule or an existing island increases. However, the desorption time decreases with temperature. Therefore, increasing the temperature does not always favour thin film growth. The diffusion length is also important in determining the island shape. If the diffusion length is large compared to the distance between the islands, the molecules will be incorporated in the nearest island. This results in correlated growth of the islands, yielding islands of similar sizes. Also, the islands will be compact in shape. If, on the other hand, the distance between the islands is large compared to the diffusion length, only molecules deposited near the island will be incorporated. This non-correlated growth will yield a broad distribution of island sizes and islands with a fractal structure.[14]

The diffusion of the molecules on the surface is very important for determining the growth dynamics. The general model of diffusion mediated growth explains the growth of the first monolayer very well. In the first stage of film growth, denoted the low coverage nucleation phase, molecules diffuse on a bare surface. These molecules might meet and from a nucleus. This nucleus might either break up again or continue to grow to form an island in a later stage. If the nucleus exceeds a certain amount of molecules, the critical nucleus size, the nucleus is stable and growth is favoured. In this phase, island growth is rare since the number of islands and their sizes are small. At a certain point in time, a significant amount of islands have nucleated. This is the intermediate growth regime. Both nucleation and island growth are occurring. This is followed by the aggregation regime. Growth of existing islands is favoured above nucleation of new islands. The monomer density becomes very small. These islands will continue to grow until they become so large that they coalesce and eventually the entire monolayer will be completed. This is the coalescence and percolation phase. Meanwhile, second and higher layer islands might start to nucleate on top of existing islands.[15]

It is also important to consider the different film growth modes possible. Depending on the surface – molecule and molecule – molecule interactions, the film can either grow layer by layer (Frank – Van der Merwe growth), in clusters or islands (Volmer – Weber growth) or as a layer plus islands (Stransky – Krastanov). For organic molecules on a non-interacting surface such as SiO_x the last is usually applicable. Pentacene usually grows in islands on top of the initial layer. Stacking of subsequent islands is often defect assisted. Because of the Ehrlich-Schwoebel barrier, the islands are often terraced.[16] However, more layer by layer like growth behaviour can be achieved if the molecular energy is sufficient to overcome this barrier.

Molecular Beam Deposition

As mentioned before, the pentacene layers used in this work were grown using two techniques, OMBD and SuMBD. These techniques are similar in the fact that they both rely on either evaporation or sublimation of the molecules and subsequent transport trough a high vacuum to the substrate. However, the details are quite different. With OMBE, the material is simply evaporated or sublimed in the vacuum. On the other hand, with SuMBD, the material is evaporated or sublimated inside a source containing a helium atmosphere. The helium and the molecules subsequently undergo a supersonic expansion into the vacuum. The important parameters of OMBD will be summarized briefly since it is a generally used technique. The details of SuMBD will be outlined more thoroughly. Finally, the techniques are compared to establish why SuMBD is such a promising and powerful technique for applications in thin film growth.

As stated, OMBD is based upon thermal evaporation or sublimation of the target material in an ultra high vacuum. To this end, some highly pure material is placed into a Knudsen cell or a similar holder which can be heated. By heating the source material, it will either evaporate or sublime.

In a Knudsen cell, an equilibrium will establish between the solid and the gas phase. A small amount of material is allowed to escape the cell into the vacuum such that this equilibrium is not affected. The escaped molecules will flow in a straight molecular beam. If the background pressure is maintained low, no collisions will occur and the molecules will continue in a straight line. By placing the substrate in the path of this flow, material will be deposited. The deposition rate is controlled by the source temperature. If the source temperature is higher, more molecules will go into the gas phase and more material will be deposited on the substrate. The temperature not only determines the deposition rate but also the energy distribution of the molecules. The molecular velocities are distributed according to the Maxwell – Boltzmann equation. Typically, the energy of the molecules is in the order of a few hundred meV. The distance from the source to the sample and the diameter of the orifice trough which the molecules escape the Knudsen cell also influence the deposition rate, but these parameters are usually fixed. This distance and the orientation of the source with respect to the substrate are also quite important in determining the film uniformity. This is because the spatial distribution of the molecular flow is quite broad and not uniform. It is common practice to rotate the sample to make sure that the deposited film is as uniform as possible. Also, a shutter is used to control the deposition time and thus the film thickness.

The second technique used is SuMBD. Just like OMBD, this technique uses a molecular beam to transport the desired material from the source to the substrate. However, this molecular beam is not a simple effusive flow as is the case with OMBD. Instead, it is a supersonic flow generated by a free jet expansion. This principle difference between the two techniques has significant implications for the properties of the beam and the deposited thin film. To generate a supersonic molecular beam, a specialized setup is required. First of all, one needs a custom built source. Typically, this is a tube made of quartz glass. Quartz is used because of the low thermal expansion coefficient, low thermal conductivity and because it is inert towards the commonly used materials. Inside this tube, an open capsule with the material is placed. A gas inlet is placed towards the back of the tube. At the front end of the tube, the nozzle is located. This is a small circular aperture with a typical diameter of 60-100 µm and a length of about 3-4 times the diameter.[17] This source is placed inside an Ultra High Vacuum (UHV) chamber. Now, to generate a free jet expansion, gas is led into the source at relatively high pressure trough the gas inlet. At this point, there is a large pressure difference between the source and the high vacuum outside. Since there is an opening in the source, the gas will flow out and expand into the vacuum. This is the free jet expansion. This expansion can be maintained if the amount of gas that flows into the UHV chamber is lower than the pumping capacity on that chamber.

Before going into details about how this free jet can be used to deposit thin films, it is useful to outline the theory of these supersonic expansions. Moreover, understanding the properties of these jets is required to understand the reasons why this technique is beneficial with respect to OMBD. Theoretically, the supersonic expansion can be treated as an isotropic expansion with negligible effects from heat conduction and viscous effects. Inside the source there is a dynamic equilibrium which is characterized by the stagnation temperature T_0 and pressure P_0. Outside the source, the pressure is the background pressure $P_b \ll P_0$. This pressure difference is the driving force for the expansion. Inside the source, towards the nozzle, the molecules will be accelerated by this pressure difference. This acceleration can be characterized by the Mach number, M. This is the ratio of the velocity of the molecules to the local speed of sound. Three distinct regimes for the expansion can be identified. In each of these regimes, the molecules have their usual thermal velocity inside the source far away from the nozzle. That is, a Mach number $M \ll 1$. However, the molecular velocities at the exit of the nozzle and beyond are dependent on the ratio of the pressures inside and outside the source. This can be quantified using the critical value G defined as:

$$G = \left(\frac{\gamma + 1}{2}\right)^{\frac{\gamma}{\gamma - 1}}$$

Here, γ is the ratio between the specific heat at constant pressure, c_p, and at constant volume, c_v. If $P_0/P_b < G$, the system is in the subsonic regime. The maximum velocity reached at the exit of the nozzle is less than that of the speed of sound, or $M < 1$. Outside the source, no further expansion will take place. If, $P_0/P_b = G$, the sonic regime is reached. At the exit of the nozzle, the molecular velocity is the speed of sound, so $M = 1$. The pressure at the exit of the nozzle is exactly the background pressure and, again, no further expansion takes place. The most interesting case is that of $P_0/P_b > G$. This is the supersonic regime. At the exit of the nozzle, the molecular velocity is still given by $M = 1$. However, the pressure of the gas is higher than the background pressure. It is given by $P_0/G \approx P_0/2$. In other words, the gas is underexpanded. Therefore, it will continue to expand until the pressure equals the background pressure. During this process the molecular velocities can increase to many times the local speed of sound. Therefore, outside the source $M \gg 1$.

In the supersonic regime, the beam assumes its characteristic features. These are shown in Figure 5. The expansion produces a shock wave. This shock wave is divided into the shock barrel and the Mach disk. The former defines the lateral dimensions of the expansion and the latter its length. If the background pressure is lowered, the shock barrel becomes more diffuse and the Mach disk will be further extended. Inside the shock waves, the so-called zone of silence is located. Here, the supersonic expansion is isolated from its environment. The theoretical foundation behind the supersonic expansion was derived under the assumption of a perfect vacuum outside the source, but were experimentally shown to hold up to a background pressure of about 10^{-3} Pa. Inside the zone of silence, the conditions are not dependent on the background pressure below about 100 Pa.[18] The theory is still valid in the zone of silence under those conditions.

It is from the zone of silence that a molecular flow is extracted by placing a skimmer in the path of the expansion. The skimmer is a conical piece of metal with a circular hole 100-1000 µm in diameter. The edges should be sharp as to not introduce a disturbance to the supersonic expansion.[18] Also, the skimmer should not be placed too close to the source to prevent a second expansion. This way, a molecular beam with well defined properties and dimensions is generated. The physical properties of the skimmed beam are the same as the final properties of a non-skimmed beam.[19] Also, during the expansion, a crossover from a continuous flow to a molecular free flow happens. In the former regime, collisions between molecules are frequent and energy transfer is possible. After the transition to the free flow regime, the number of collisions decreases dramatically. Because of this, the kinetic processes freeze out and a non-Boltzmann distribution of the population of the energy states occurs. Most importantly, the rotational and vibrational degrees of freedom are cooled down. A final important property of the molecular beam is the very narrow velocity distribution, both parallel and perpendicular to the beam. If the final temperature of the beam is lower, this distribution becomes even narrower. A lower final temperature can be achieved by increasing the pressure gradient, giving a better expansion. This fact is useful in applications such as He atom diffraction experiments.

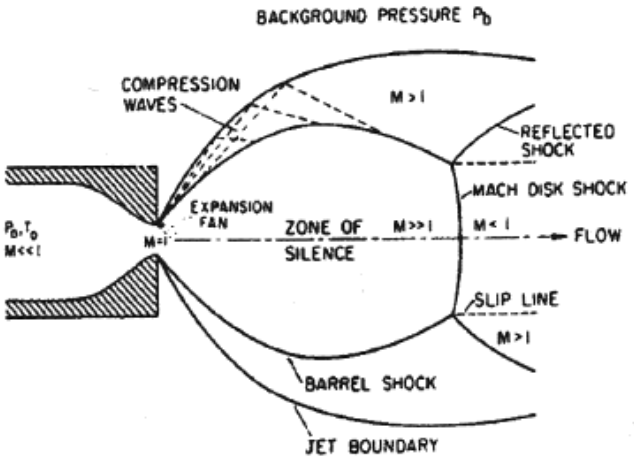

Figure 5: A schematic representation of the features of a continuous free jet expansion. Image from 20.

The general properties of the supersonic expansion have been outlined above, but a final step is required to be able to use this technique for film deposition. This is because the above method requires a high pressure in the source. Typical organic molecules suitable for applications decompose well below the temperature where their vapour pressure would be sufficient to do SuMBD. Fortunately, there is a good method to get around this problem. This is the seeded supersonic molecular beam. A seeded beam is a beam in which the target material is present in small quantities. If the number of seeded molecules is less than one in thousand, the expansion of the gas is not affected significantly.[17] In practice, only about a tenth of this amount is present. To generate the seeded beam, the target material is evaporated or sublimed inside the source while the carrier gas flows in from an outside supply such as a gas bottle. Even though the overall expansion is unaffected, the use of a seeded beam has some important consequences. Most importantly, if a heavy molecule, such as pentacene, is seeded in a light carrier gas, such as helium, the final velocity that the heavy molecules reaches much higher values than in a beam of the pure material. In other words, the heavy molecules are extra accelerated by the carrier gas. This effect is often referred to as aerodynamical acceleration. The opposite effect is also possible when a light molecule is seeded into a carrier gas of a heavy molecule. However, there is always a difference in the final velocity of the components. This is known as the velocity slip. Likewise, there is a difference in the final temperature, or a temperature slip. Also, a broader distribution of lateral velocities for the carrier gas causes a relative concentration of the seeded molecules in the centre of the beam after it passed through a skimmer.[21] Another interesting effect that occurs for non-spherical molecules is that they will align with the long axis parallel to the beam direction.[22] All of the above properties of the seeded molecular beam are a result of many collisions between the molecules of different species.

The kinetic energy of the seeded molecules can be controlled by changing the expansion parameters. The two most important parameters are the temperature at the nozzle and the carrier gas pressure inside the source. The former is controlled by heating the front of the source with a special tantalum heating wire. In practice, this parameter is kept constant. However, the carrier gas pressure is very important. The higher the pressure inside the source, the higher the pressure gradient driving the expansion. Naturally, this results in a higher kinetic energy for the molecules. The maximum kinetic energy that can be achieved depends on the carrier gas and the SuMBD setup, as will be seen below. However, unlike OMBD, the deposition rate can be varied independently by changing the temperature of the material inside the source. This is done using a separate tantalum foil heater. A higher temperature in the source means that more of the target material evaporates or sublimes, hence more will be seeded in the beam.

The SuMBD setup requires a purposely build source, as outlined earlier. However, the UHV chamber itself is also quite important. First of all, a typical SuMBD setup consists of a series of three connected chambers. The first one, the expansion chamber, contains the source. It is crucial that the pumping speed at this chamber is as high as possible, since the background pressure should be kept low enough to not disrupt the expansion. The shape of the first chamber is also important because reflected shock waves could potentially disrupt the beam if it was not designed properly. The first and second chamber are connected via the skimmer in front of the source. This chamber should also be pumped adequately, but the material influx is not as high as in the first chamber. This chamber is connected with the deposition chamber trough a second skimmer. This second skimmer is usually a few millimetres in diameter and it is used to align the beam with respect to the sample. In the deposition chamber, the sample holder positions the substrate in the path of the beam. The substrate remains fixed throughout the deposition.

SuMBD offers some benefits over OMBD as a method for growing thin films. The most important one is the much higher kinetic energy of the molecules. When the molecules arrive at the surface, much of their kinetic energy is transferred to the internal degrees of freedom. However, part of the kinetic energy is conserved and the therefore the molecules will diffuse with hyperthermal velocities over the surface. Substrate phonons assure momentum conservation during adsorption.

Because of this, the molecules can diffuse much further over the surface before re-evaporating for the same surface temperature. Also, part of the energy is transferred to the substrate, or to an existing part of the film causing local annealing. This could also contribute to the higher quality of SuMBD grown films. Another, more subtle, benefit is the fact that the kinetic energy of the molecules can be changed independently from the deposition rate. This is useful, because at higher deposition rates the film growth parameters can change as well. The fact that the beam is collimated is also advantageous because far less material is wasted this way. On the other side, a lot of carrier gas is used and the depositions are typically much slower for SuMBD growth.

Microbalance and Time of Flight Mass Spectrometer

A quartz microbalance was used to monitor the film thickness in both the SuMBD and OMBD setup. This is a very well known technique based on the piezoelectric properties of quartz crystals. A material is defined to be piezoelectric when a voltage applied to the crystal results in a structural deformation and vice versa. The crystal will therefore oscillate under an AC voltage. In the microbalance, a small quartz crystal with a specific shape is used. Standing shear waves are generated in this crystal by the application of the AC voltage. The frequency of this mode can be determined with very high precision and will scale with the mass of the crystal. These two properties make it suitable for the measurement of the deposition rate. If material is deposited on the microbalance, a change in frequency will occur, which can be translated to the mass of the deposited material. If the density and the sticking coefficient of the material on quartz are known, the flux of molecules can be determined. This can in turn be converted to the growth rate of the film on the sample. It might differ from that on the quartz crystal because of different sticking coefficients.

To determine the velocity and the flux of molecules impinging on the substrate during SuMBD depositions we employed Time of Flight Mass spectrometry (ToF-MS), which is also relatively simple. Normally, it is used to identify the kind of molecules present in a sample. However, in this case it is used to characterize the kinetic energy of the seeded molecules as a function of the applied helium pressure. To measure the time of flight of the molecules, they are first photoionized. This ionization is soft so the molecules generally do not disintegrate. This is beneficial, because this fragmentation process would make the data analysis significantly more difficult. After ionization the molecules are accelerated by a series of potential differences and finally arrive at a detector. By synchronisation with the laser, the exact time of flight can be calculated. If the molecular mass is known, the exact velocity, and thus the kinetic energy, of the molecules before ionisation can be determined. Generally, the signal is integrated over time, to include many individual molecules. The peak position of the resulting distribution will give the average kinetic energy, while the area under the curve is proportional to the amount of molecules and hence the flux. Therefore, ToF-MS could also be used to determine the deposition rate. However, since the cross section for ionization is different for each molecule quantification is difficult. Impurities in the beam can be detected if peaks other than those of the carrier gas and seeded molecules are present.

Atomic Force Microscopy

Atomic Force Microscopy (AFM) is used to analyze the deposited films. A schematic representation of the AFM is shown in Figure 6. In AFM the motion of a cantilever, due to forces acting on the tip, is measured by detecting laser light reflected of the back of the cantilever with a position sensitive photodetector. This technique is very powerful for imaging the surface of an object. It is a very well known technique, therefore it will be discussed briefly. Only the details of two important operating modes, Lateral Force Microscopy (LFM) and Transverse Shear Microscopy (TSM), will be discussed in more detail. AFM is one of the two most important scanning probe techniques, the other one being Scanning Tunnelling Microscopy (STM). AFM is chosen because it works for insulating surfaces whereas STM requires a conducting surface. The most important reason, however, is the fact that the aforementioned modes are especially powerful for pentacene thin films. They can yield information which goes beyond the surface topography.

An AFM image can be obtained it two principal ways. The first is called tapping mode and the second contact mode. Tapping mode is the most commonly used method for several reasons. First of all, it is faster than contact mode. Also, because there is virtually no contact between the tip and the sample, the sample will not get damaged as easily as in contact mode. Moreover, because of the little contact in tapping mode, the tip will not readily acquire contaminants from the surface which greatly increases the lifetime of the tip. In tapping mode, the cantilever is driven to oscillate near its natural resonance frequency by a vibrating piezoelectric element in the tip holder. When the tip approaches the surface, forces such as the Van der Waals forces start acting on the tip. This change results in a shift in the resonant frequency of the tip and therefore a deviation of the oscillation amplitude from the set point. A feedback loop adjusts the height of the tip above the sample to counteract the change in amplitude. The servo motion is translated to an actual map of the sample. It is also possible to measure the phase shift of the oscillation with respect to the driving oscillation. This gives a so called phase map. The phase contrast is due to differences in the amount of energy dissipated during oscillation.

In contact mode, as the name suggest, the tip is operated in contact with the surface. This mode is less convenient for obtaining topography images of soft samples, such as organic crystals. This is because the drag from the tip on the sample can easily damage both the sample and the tip. However, by applying only a mild force on the cantilever, this drawback is minimized. In contact mode AFM, the tip is brought down to the sample until contact is achieved. This is measured by the bending of the cantilever. When a force is applied to the tip by the sample, the cantilever bends up or down. The bending of the cantilever is used in a feedback loop as described before. A change in height of the sample results in a different force. The servo will move to counteract this force, such that the set point signal on the detector is maintained. The movement of the servo is again related to the sample topography.

In contact mode, not only the height can be determined. Also, the twisting of the cantilever can be detected by lateral displacement of the laser spot on the detector. This twisting is due to lateral forces acting on the tip. The AFM mode depends on the scan direction, as shown in Figure 6. If the fast scan direction is perpendicular to the long axis of the cantilever, it is referred to as LFM.

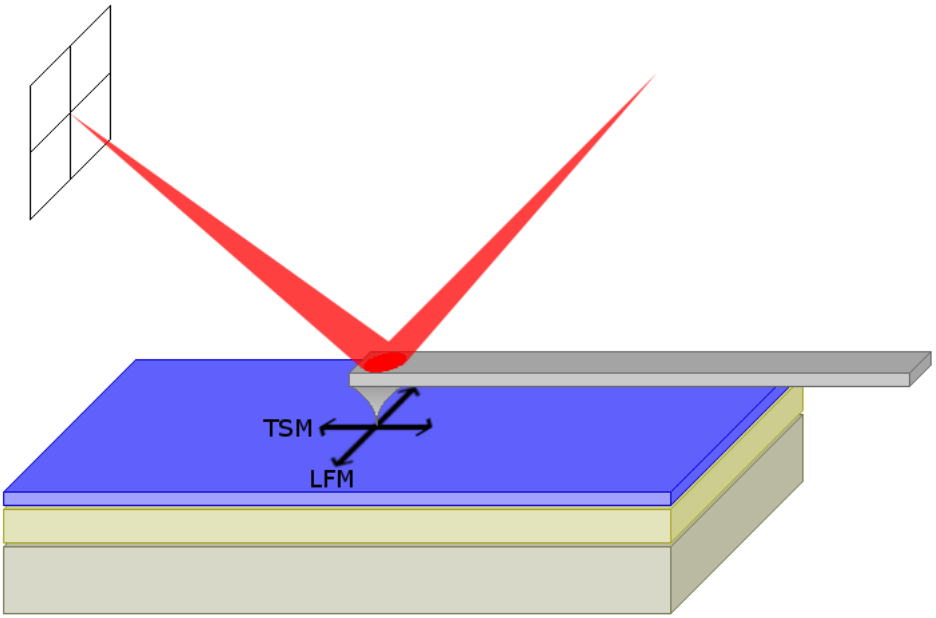

Figure 6: A schematic representation of the AFM. The motion of the tip is determined using the reflection of a laser. Bending and twisting of the cantilever will cause the reflected laser light to fall on a different part of the detector. In contact mode, if the fast scan axis is perpendicular to the long axis of the cantilever the mode is refered to as LFM, if they are parallel it is referred to as TSM.

This mode is the conventional mode, where the tip moves in a 'stick-slip' kind of fashion over the surface. While the cantilever is scanned over the surface, the tip will stick to the surface due to friction forces. If the applied force is large enough to overcome the friction, the tip will move until it sticks again. This way, the cantilever is always twisted in the same direction with respect to the cantilever motion. The trace yields a clockwise rotation and the retrace will yields a counter clockwise rotation. However, the degree of twisting is dependent on the friction. Thus, an LFM image shows the different friction regimes. For a chemically homogeneous surface, a major contributor to the friction is the amount of defects in a certain area. Higher friction regimes often correspond to regions with an increased defect concentration. The friction itself is proportional to the difference between the trace and retrace signals, which is always positive.

The second operating mode of contact AFM is TSM. In this mode, the fast scan direction is parallel to the long axis of the cantilever. Clearly, the main friction forces are now unable to twist the cantilever as they are directed parallel to the cantilever. However, it was shown in 1996 that there can be a twisting of the cantilever in this mode.[23] This effect is small, about ten times smaller that of conventional LFM, but non-zero.[24] Later, in 2006, it was shown that this AFM mode is also very useful for the investigation of pentacene thin films.[25] In several subsequent publications the details of TSM were further investigated using pentacene thin films and single crystals.[6, 24, 26] In particular, the TSM signal was shown to correspond to the crystalline orientation of the film. This enables the visualization of the grain structure of film. In the topography, a featureless layer is observed because the height is uniform, but in TSM the contrast shows that this layer is actually build up of many different grains. The TSM contrast was shown to be correlated with the crystallographic orientation of the grains. The trace can yield both a clockwise and a counter clockwise twist, but the retrace always yields the same twist in the opposite direction. The TSM signal is defined as the trace minus retrace signals, similar to the friction, but it can be either positive or negative. In Figure 7, the TSM signal as a function of crystallographic direction is shown for pentacene. Using this map, the crystal orientation of each grain in pentacene thin films can in principle be determined.

Even though the TSM signal is known to correspond to the crystallographic direction, the exact origin of the contrast is still under debate. In 2010, a comprehensive study on the details of TSM was published.[26] To establish the differences and similarities between the TSM and LFM signals, their behaviour as a function of temperature and scan speed was determined. In LFM, the signal diminishes with temperature. This is because friction is due to thermally activated hopping of the contact atoms. In TSM, on the other hand, no temperature dependence is measured. A similar observation is made by changing the scan velocity. The LFM signal depends on the scan speed in the lower velocity regime, again due to activated hopping, and is constant for velocities where the thermal activation is no longer relevant. The TSM signal is not dependent on the scan speed. For this reason, the TSM signal was believed to be of an origin very different from friction. Instead, elastic shear deformation forces were proposed to be the physical origin of this contrast. That is, the tip induces deformations on the sample surface, possibly resulting in a shear force acting on the tip. Due to the crystalline anisotropy, this shear force is non-zero for certain directions. Since the elastic constants of the pentacene crystal are unknown, those for anthracene were used to test this model. The result can be seen in Figure 7 A. The solid line denotes the fit and it is in good agreement with the data. However, the fit is very sensitive to the values used for the constants, as demonstrated by the dotted line. Here, one constant has been increased 60%, resulting in a very different curve.

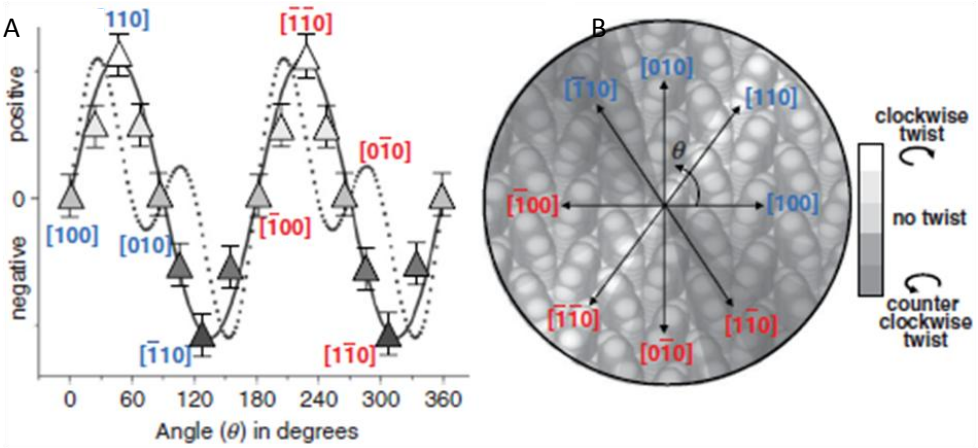

Figure 7: The TSM signal as a function of the angle (A). A period of 180° is observed. The solid and dotted lines are predictions from a model based on elastic shear forces, used to explain the TSM signal. The figure shows the different crystallographic directions and their corresponding TSM signals onto of a model of the crystal. Image taken from 26.

In 2010, another paper on TSM was published.[27] In this case, crystals of potassium hydrogen phthalate (KAP) were used because the elastic constants of this material are already known. It was found that the agreement with the above model was very poor. Even the number of crystallographic directions for which the TSM signal is zero did not match. Therefore, the authors devised a new model based on non-linear anisotropic friction. The agreement of the experimental data with this model was much better. Also, it fits the experimental trend obtained on pentacene crystals. In this model, the TSM signal is assumed to be proportional to the transverse component of the friction vector. In other words, the TSM signal is actually due to friction effects. A good way to visualize this is to look at a rigid textured surface. In certain directions, parallel trenches with nanoscopic spacing are present. If the sample is scanned at an angle with respect to these trenches, the tip is pushed outward because it tries to follow these troughs. The catch here is that the action of different trenches cannot simply be added in a linear combination. Instead, significant non-linearities are present. Therefore, a complicated model is necessary. The proposed model is also in agreement with the fact that the TSM signal is not dependent on the scan speed and the temperature since the action of the trenches on the tip is not thermally activated. One final remark with respect to the TSM signal, is that it is not a constant at the atomic length scale. Periodic variations, corresponding to the atomic length scale, can be observed in very high contrast images.

Etching

As mentioned in the introduction, the main part of this work was devoted to the study of defects in pentacene thin films. To this end, the thin films were etched using diluted sulphuric acid. This kind of experiments has been performed for OMBD grown pentacene thin films.[25] The goal is therefore to compare these results with SuMBD grown thin films. In the article by Daniel Frisbie's group, etch lines have been observed by AFM after a 5-10 s etching step. These lines have only been observed in the second ML. Also, they appear in groups of parallel lines which are confined to the high friction regions of the second ML. These lines are actual grooves in the film as they are visible in both the topography and the LFM images. The lines are visible in Figure 8 A and B. The exact origin of these lines it not certain, but two proposed models are shown in Figure 8 C and D. A stress build up due to an epitaxial mismatch with the first ML is believed to be the cause of the formation of these defects.

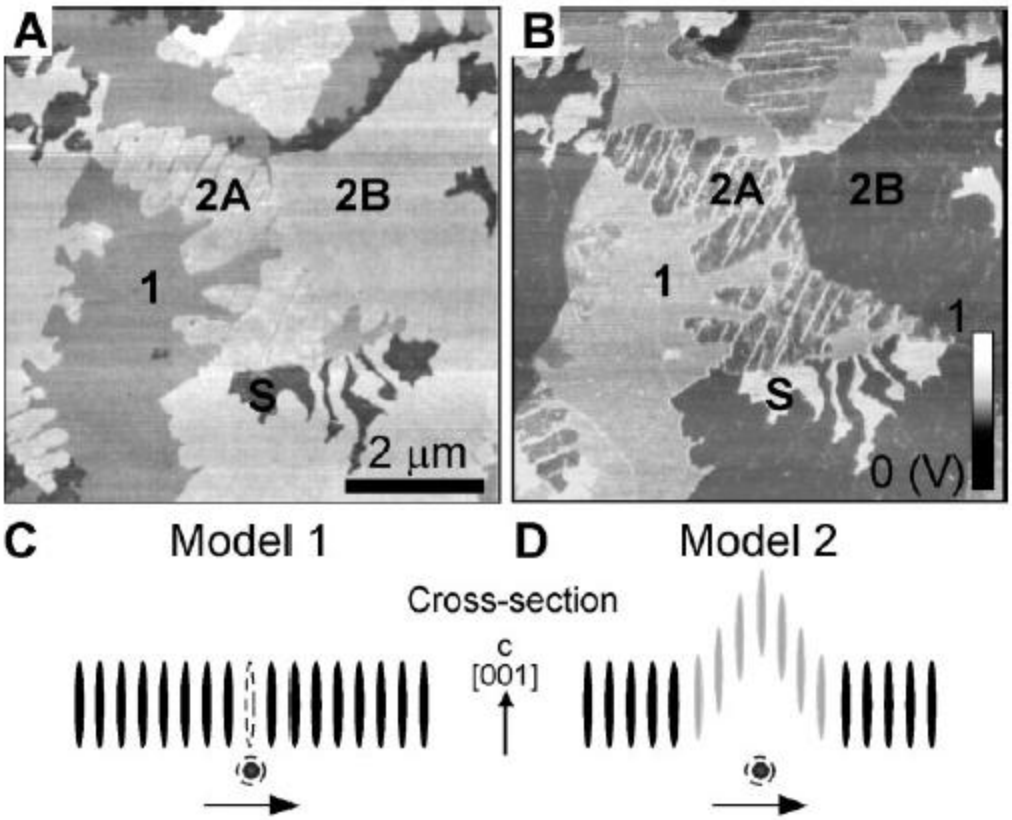

Figure 8: Dislocation made visible by AFM on an etched sample in topography (A) and LFM (B). Two models for the type of defects are also shown (C and D). Image taken from 25.

These defects can be visualized by a short etching step because the weakest bound molecules are first attacked by the acid. In this case, the molecules around the dislocation lines are weakly bound due to the very presence of the defect. If the etching continues, other molecules will also begin to be affected significantly. These could be molecules present at the step edges and eventually the entire pentacene film will be etched away.

Experimental

In this chapter, the details of the various techniques used and the different experimental setups are discussed. The first two sections will cover the wet chemistry used for the cleaning of the SiO_x substrate and the etching procedure. The third section will cover the MBD setups employed. This will include the characterization of the properties of two new sources for the SuMBD setup. The last section will briefly introduce the two AFM setups used in this work.

Substrate cleaning

The substrate used was a silicon wafer with a 290 nm thick thermal silicon oxide layer (Silicon Quest International, USA). The surface roughness and hydrophobicity were previously determined. From AFM in tapping mode, a low root mean square roughness of about 0.5-0.6 nm was found. The surfaces were moderately hydrophobic, as concluded from the contact angle of water, which was about 60°. The substrate was cleaned using a standard technique capable of removing most impurities from the sample. The SiO_x layer present on the substrate is unaffected and not modified.

After the silicon wafer has been cut into pieces of the appropriate size, typically about 13 x 13 mm, the dust is removed by blowing with argon from a gas bottle. Subsequently, the sample is cleaned in an ultrasonic bath, first in acetone followed by 2-propanol. Both sonication steps are approximately 15 min and are followed by quick blow drying using argon. The sample holders were treated using the same procedure. The cleaned samples were transferred into the UHV system as quickly as possible. Inside the SuMBD, the samples and holders were heated to about 240°C overnight to remove any water and other volatile contaminants that might still be present. The samples were allowed to cool down to room temperature before deposition.

During this work, two depositions were also carried out on MgO. A single crystalline sample of 5 x 10 mm, polished on one side, was used. A special cleaning method is required for this material, to be able to remove any carbon based contaminants from the surface. To this end, the samples were placed in an UHV chamber usually used for Pulsed Laser Depositions. The sample was heated at 650°C for one hour in a 10^{-6}-10^{-5} mbar oxygen atmosphere. The oxygen is required to react with the impurities on the sample such that volatile species such as CO_2 are formed. After this cleaning step, the samples were transferred to the SuMBD setup within 15 min and annealed in vacuum once more to remove any contaminants deposited during transfer.

Etching

The etching procedure used was taken from literature[25] and is quite straightforward. First, a 2:1 H_2O:H_2SO_4 solution was prepared. The water used was highly pure MilliQ water. The sample, with the pentacene layer, was immersed into this solution for a specified amount of time, usually 5-10 s. Then, the sample was neutralized and cleaned by thorough immersion in water followed by argon blow drying.

Note: this is the procedure taken from literature which was used as such in this project. However, no results were obtained using this method. After contacting the group of Frisbie about this discrepancy, we learned that the article gives an incomplete recipe. Additional steps are required for a good visualization of the defects. First of all, a cold solution of sulphuric acid is recommended. If the solution is still warm from the mixing process, the revealed lines might heal. Also, after the initial immersion in water, two additional cleaning steps are required, namely rinsing with 2-propanol and ethanol. Both rinsing steps are 10 s, and serve to remove reacted material deposited on the sample and to clean out the trench at the dislocation lines. A final water rinse and blow drying conclude this procedure.

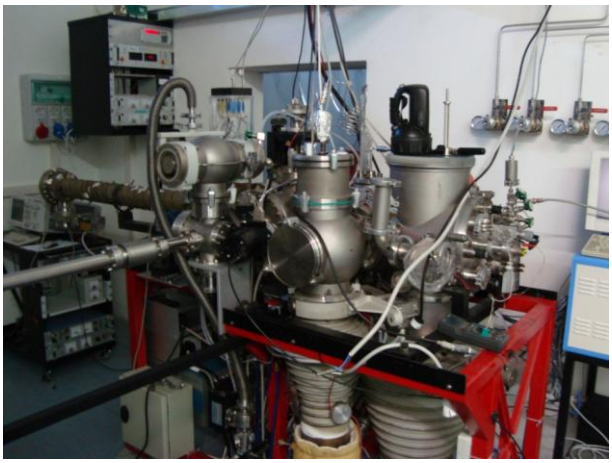

Figure 9: The SuMBD setup in Trento, Italy. The first chamber containing the source is located on the right side. The diffusion pumps are visible in the front and the elongated part at the back is the ToF.

MBD

The OMBD setup used was a fairly standard setup with a bell shaped vacuum chamber. This chamber was installed in a nitrogen glove box to avoid problems with water and oxygen. The setup was build by De Jong B.V. and installed by local engineers. The pressure inside the chamber was well below 10^{-6} during deposition. Pentacene was evaporated from a Knudsen cell at a rate of about 0.01 nm s^{-1}.

Two different SuMBD setups were used. The first, located in Trento, Italy, is shown in Figure 9. This setup was used to characterize two new sources. The setup of this SuMBD consists of three UHV chambers, namely the expansion chamber, the differential pumping chamber and the deposition chamber. The first two chambers are equipped with two large diffusion pumps providing the large pumping capacity required for SuMBD. Both pumps are backed by a roughing pump. The deposition chamber is fitted with a load lock and it is pumped by a turbo pump. The source is attached to a flange together with the gas inlet, the heating system and the thermocouples. This way, the source can easily be removed, for example to refill the material in the source. A microbalance and a ToF-MS are present for the beam characterisation. For the ToF, the molecules are photoionized by the fourth harmonic of an Nd:YAG laser. The wavelength is 266 nm and the pulse time and frequency are 15 ns and 8 Hz. There is also the possibility to measure the film thickness using ellipsometry.

Two new sources were made in Trento. These had approximate nozzle diameters of 120 and 100 µm, respectively. Both sources were characterized using the ToF-MS, that is the kinetic energy of the molecules was determined as a function of the pressure in the source. The region attributed to pentacene in a typical ToF spectrum is shown in Figure 10. A single cycle of photoionization and detection usually yields only a few counts. Therefore, the integrated intensity over many individual cycles is shown. The time of arrival is the difference between the ionization by the laser pulse and the subsequent detection of the ions. Five individual peaks can be recognized, as numbered in Figure 10. The first peak is due to pentacene that has been deprotonated in the ionization processes. The second peak is the main peak of pentacene. The third and forth features are due to pentacene molecules containing one or two heavy atoms, ^{13}C or sometimes ^{2}H. Peak four can also be due to hydrogenated pentacene, 6-13-Dihydropentacene. This is a common impurity in the pentacene source material which has a much higher vapour pressure than pentacene. It can easily be eliminated by leaving the system running without depositing. Therefore it is common practice to do this after the source material has been refilled. The last peak, number 5, is due to any pentacene present in the background pressure. The initial velocity of these molecules is their thermal one in any direction. Thus the peak is broad and the time before arrival is much longer.

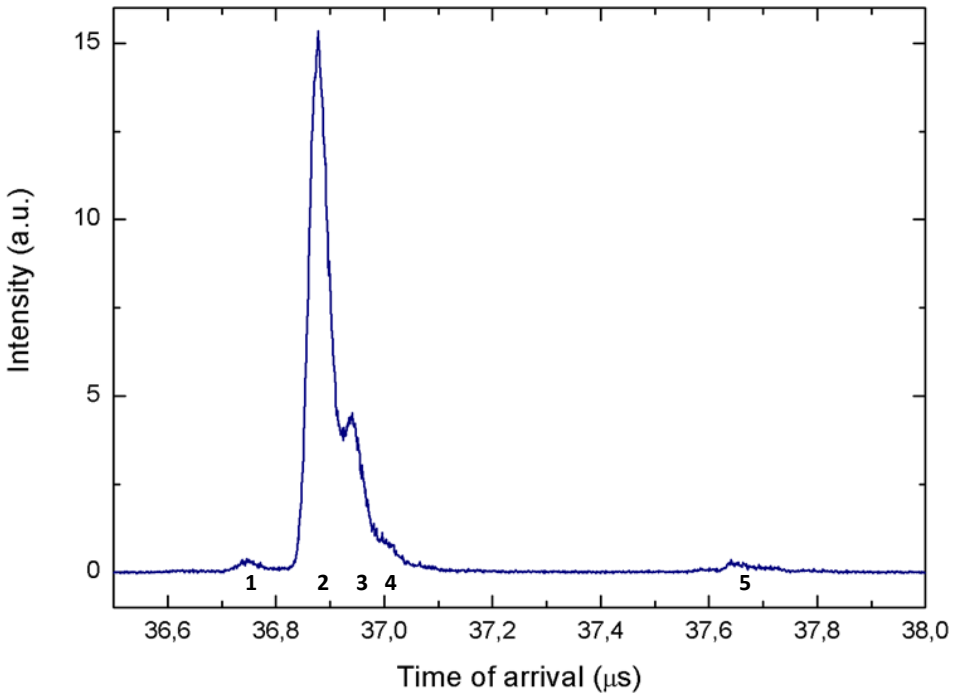

Figure 10: A detail of the ToF spectrum where pentacene is detected. The five peaks are identified in the text.

From the ToF data, taken at a series of different helium pressures, the kinetic energy of the molecules as a function of pressure can be determined. The resulting curves are shown in Figure 11. It can be seen that a higher pressure can be reached with the second source. This is because the diameter of the nozzle is smaller and therefore the flux of helium is lower for the same pressure. Since a higher pressure can be reached, a slightly higher kinetic energy can also be achieved. The fit to both data sets has the form $y = y_0 - A_1 e^{-x/t_1}$. All fit parameters are positive. The parameter y_0 is the most interesting, as it gives the maximum kinetic energy that can be achieved with the source. It was found to be about 6.6 and 6.8 eV respectively. This is in agreement with theory.[28]

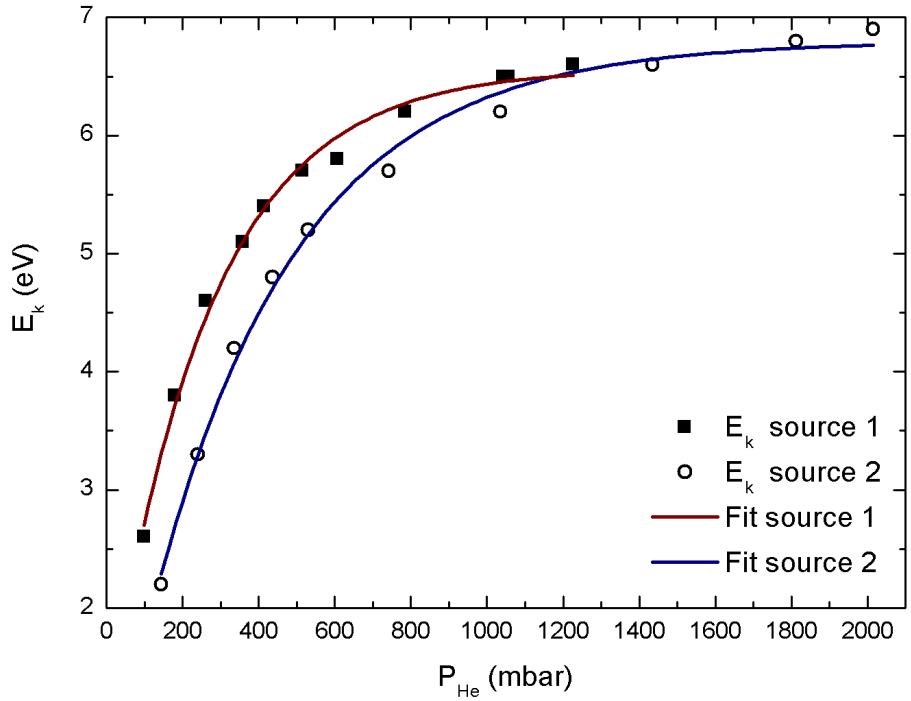

Figure 11: Kinetic energy of the pentacene molecules plotted as a function of applied pressure in the source. Source 1 and 2 are the sources with a nozzle of 120 and 100 μm in diameter, respectively.

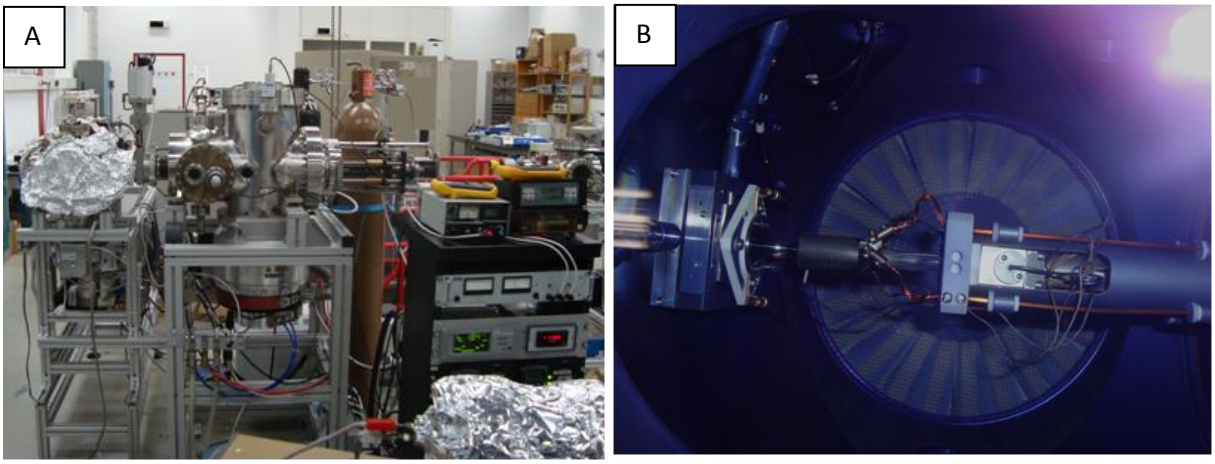

Figure 12: The SuMBD setup in Groningen (A) and the source in the first chamber (B). The first chamber containing the source is located in the center of the first photo. The large turbomolecular pump is visible below the first chamber. The deposition chamber is the one wraped in aluminium foil. The quartz glass source is visible in the center of the second photo, but the front part is covered by the heating element. The skimmer is located at the left side.

The second setup, located in Groningen, is shown in Figure 12 A. Also, the source located in the first chamber is shown in Figure 12 B. This setup was used to grow the pentacene thin layers investigated in this work. The basic setup is the same as in Trento but it is a more recent machine and therefore several details are different. First of all, the chambers are pumped down by turbomolecular pumps instead of diffusion pumps. The pumping capacity is somewhat higher. Also, the helium is supplied from a gas bottle and not from a gas line. The deposition chamber does not have a load lock, which is a disadvantage of this system. The entire deposition chamber has to be vented in order to introduce or remove samples. A Vat valve is located between the second chamber and the deposition chamber so only the deposition chamber has to be vented. The sample holder is more convenient in this new machine, as it holds four samples at a time. However, due to the nature of the beam, only one sample can be grown at a time. The holder can be rotated to allow for different angles of incidence. It can also be heated or cooled to control the substrate temperature. This system is equipped with a microbalance to determine the rate of the deposition. However, there is no possibility to do ellipsometry or ToF measurements. Since the sources were calibrated in Trento and the geometries of the chambers are analogous, we assume that these calibrations are also valid for operation in Groningen.

AFM

In this work, two different AFM setups were used for the same kind of measurements. The first was a Scientec 5100 from ScienTec. The other setup was a NanoScope IIIa from Veeco, Digital Instruments. Both AFMs were operated in air. Tapping mode images were obtained using a silicon nitride cantilever with a tip radius less than 10 nm and a force constant between 25 and 75 Nm^{-1}. Contact mode images were taken with Veeco silicon tips with a radius of about 2 nm on a triangular silicon nitride cantilever. The spring constant of this cantilever was 0.58 Nm^{-1}. The data was processed using Gwyddion 2.19.

Note: in the course of this project, we discovered that the calibration of the Scientec 5100 AFM was not correct. The in plane dimensions were a factor 2 too large and the out of plane direction was a factor 1.5 too large. That is, a supposedly 10 x 10 μm^2 images was actually a 5 x 5 μm^2 area. The images taken on this AFM are reported in this work with their original wrong dimensions. These micrographs are marked with an asterisk (*). They are of the same quality as the ones collected with the Veeco instrument.

Results and discussion

In this work, the defect structures in thin films of pentacene were investigated. The main research question was whether there is an intrinsic difference between the defects in thin films grown with the conventional technique of OMBD and the novel technique of SuMBD. From earlier experiments it is known that the quality of SuMBD grown films is significantly better because there are less grain boundaries.[29] However, it is not known if the defects are different or simply less abundant. In either case, these details could shed new light on the principles behind the technique of SuMBD as well as help to improve pentacene thin film quality for future device applications. In this section, the results of the etching experiments will be outlined first. This will be followed up by a number of other interesting observations on the investigated films.

Etching of pentacene thin films

To investigate the line defects in the pentacene thin films, the samples were etched using a diluted sulphuric acid solution. The procedure outlined in the previous chapter was followed closely. A significant number of different samples were deposited and etched. The thickness of the samples was chosen such that a significant amount of the second layer of pentacene was exposed, which was checked before etching using the AFM. Having exposed second layer islands is important, since the etch lines were only found in this particular layer.[25] After etching, AFM was used to confirm the presence of any etching lines. Contact mode AFM was used in all cases since these lines should be best visible in the contact mode topography and LFM images.

The first set of experiments involved SuMBD grown films. Both films grown at high and low energy were used for comparison. A total of six films were grown for the purpose of etching, three at low and three at high energy. For four of these samples, the recommended etching time of 10 s was used. The other two were etched for over one minute. The film thickness was varied slightly between different depositions to achieve an ideal film thickness of about 1.5 to 1.7 ML. Unfortunately, not a single etch line was found in any of these pentacene films. This is surprising because in the article by Frisbie's group[25] they appear to be very common. In fact, the authors reported to have found them in every area with higher friction. Moreover, such high friction areas have been observed in the samples investigated here. Contrast in the friction was very common in the AFM images. This was the case both before and after the etching step. This excludes the possibility that the entire defected areas could be etched away. Also, this makes the possibility that the line dislocations were simply missed in the AFM images unlikely. Moreover, given the number of samples and over 10 AFM scans with different image sizes it is improbable that the etch lines were simply overlooked.

Only samples etched for one showed more than an increase in contaminants as the only visible effect of etching. Representative AFM images are shown in Figure 13. It can be seen that both AFM images, taken on the same sample before and after etching respectively, feature some islands with a rhombohedral shape. Before the etching step, the edges of these islands are quite straight. The edge indicated with an arrow is a prime example of this. After etching, the edges of a similar island appear to have withered away. Again, a good example is indicated with an arrow in the figure. This observation shows that the sulphuric acid solution is capable of etching away the pentacene molecules.

At this point, there are two possible explanations for the absence of the dislocation lines in the etched samples. Firstly, this could mean that the defect structures in the SuMBD grown samples were significantly different, and these dislocations were not formed in these films. On the other hand, the possibility of another problem with the etching procedure could not be excluded. To confirm the results obtained with the SuMBD grown samples, another six samples were grown using conventional OMBD. Films of three different thicknesses were deposited, with two samples grown simultaneously for each thickness. Samples with the same thickness were either etched 5 or 10 seconds. Again, not a single dislocation line was found after etching. This confirmed the suspicion that there was something wrong with the etching procedure.

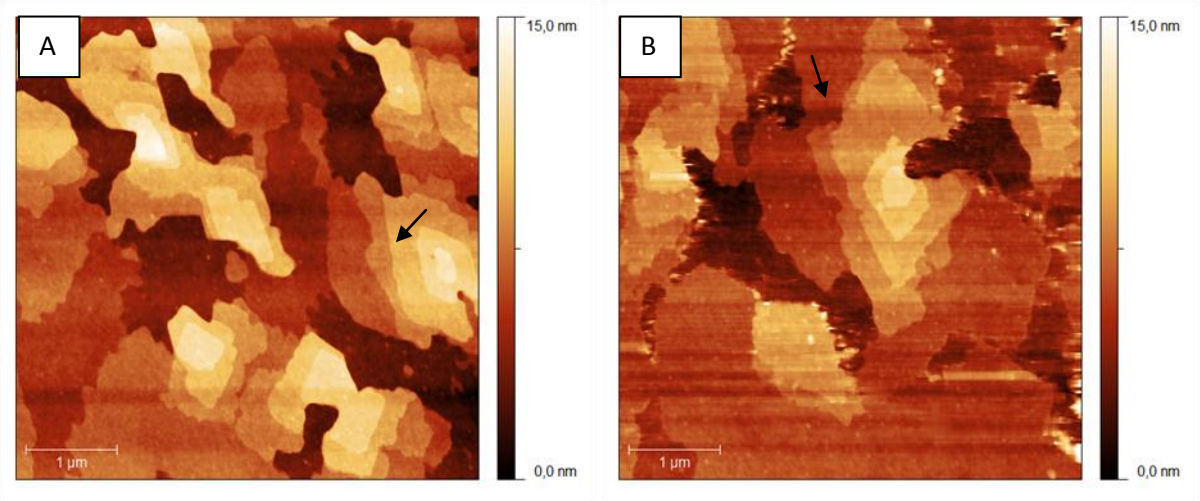

Figure 13: Two AFM images of the same sample before (A) and after (B) etching. The arrows denote a straight edge before etching and a similar edge after etching that appears to be affected by the acid. Deposition time: 61 min, kinetic energy: 6.8 eV and etching time: 1 min. *

Indeed, direct contact with the Frisbie group confirmed that the procedure as reported in the article was not quite optimized to visualize the dislocations. A few important points that could be relevant to make the defect lines actually visible were not known. Their latest investigation resulted in various suggestions. First of all, the etching solution could be made stronger, that is a 1:1 solution of Sulphuric acid and water, for better results. It is also important to let the solution cool before etching. The heat produced upon mixing water and the acid can potentially cause the defect lines to heal while etching. If this is the case, no lines will be visible in AFM images. Also, the cleaning of the sample after etching should be more elaborate. Instead of using only two water rinsing steps, the sample should also be rinsed with isopropyl alcohol and ethanol. These two rinsing step should take approximately 10 s each and should follow the first water rinse. The film is stable to the organic solvents during these short rinsing times but any contamination from reacted pentacene on the surface will be washed away. Moreover, these extra steps clean the trenches where the dislocations are present. This way, they will be much more visible on the AFM images.

Unfortunately, this news came too late to be applied in this project, so it is clear that these experiments should be done once more using the new details outlined above. Currently, it is not possible to conclude anything meaningful about the presence of line dislocations in the second layer of pentacene thin films grown using SuMBD. Only some circumstantial evidence base on LFM contrast analysis, discussed in the next section, is available. If these defects are indeed found, it is also useful to address their abundance. whether they occur more or less at the same frequency in films grown with SuMBD and in films OMBD, or with a significantly different frequency.

LFM, TSM and phase contrast analysis

Fortunately, the lack of etch lines was not the only interesting observation on the films grown. For both the AFM images taken in contact mode and tapping mode, the most remarkable features are not revealed in the topography images. Rather, the phase maps for tapping mode or the LFM and TSM maps for contact mode show some interesting contrast characteristics. To discuss these features, several representative AFM images will be shown and compared.

First, several observations on contact mode images will be discussed. Five groups of images will be presented, each containing a LFM and a TSM image of the same area. As discussed earlier, the TSM contrast can be related to the crystalline orientation of the pentacene domains. This is a quite well known feature of these TSM images.[26] In fact, this contrast makes TSM such a valuable tool to unravel the crystallinity of thin films of pentacene. It enables observation of the domain sizes even in a fully coalesced layer. However, the signal is quite weak, especially when compared to the regular friction contrast. On the other hand, contrast in LFM is not well studied for pentacene thin films.

As far as we are aware, there is only a single paper in literature describing LFM contrast in the second layer of pentacene films.[25] In that work, the contrast is associated with the existence of line dislocations which only appear in high friction domains.

The first set of AFM images is shown in Figure 14. The left images are the topography images associated with the LFM and the TSM signals on the right. The corresponding topography images are both shown for convenience since they do not overlap properly due to thermal drift. This sample was grown by SuMBD in two subsequent depositions at high energy such that the total film thickness is less than one monolayer. The AFM micrographs illustrate two important characteristics of LFM and TSM, which are relevant in the discussion of the micrographs of the other samples. The first feature is marked with arrow 1. In the topography image, the island is featureless. However, a clear contrast difference in the TSM signal shows that the crystalline orientation of the two halves of the island is not the same. Also, the LFM contrast shows a feature best described as a crack on the boundary of the two areas with different crystalline orientations. Together, these two observations show that the island consists of two grains with different crystalline orientation linked by a grain boundary. Another important characteristic is indicated by arrow 2. This island appears uniform in the LFM image, but the TSM image shows that this island is actually build up of two different domains. Because there is no grain boundary visible in the LFM, it seems unlikely that this island is actually the result of two coalesced islands. Therefore, this must be a naturally occurring defect. Perhaps it is a twin boundary with a well defines symmetry relation between the two sides. Such a symmetric twin boundary could be formed randomly or it could be induced by a substrate defect during the growth of the island.

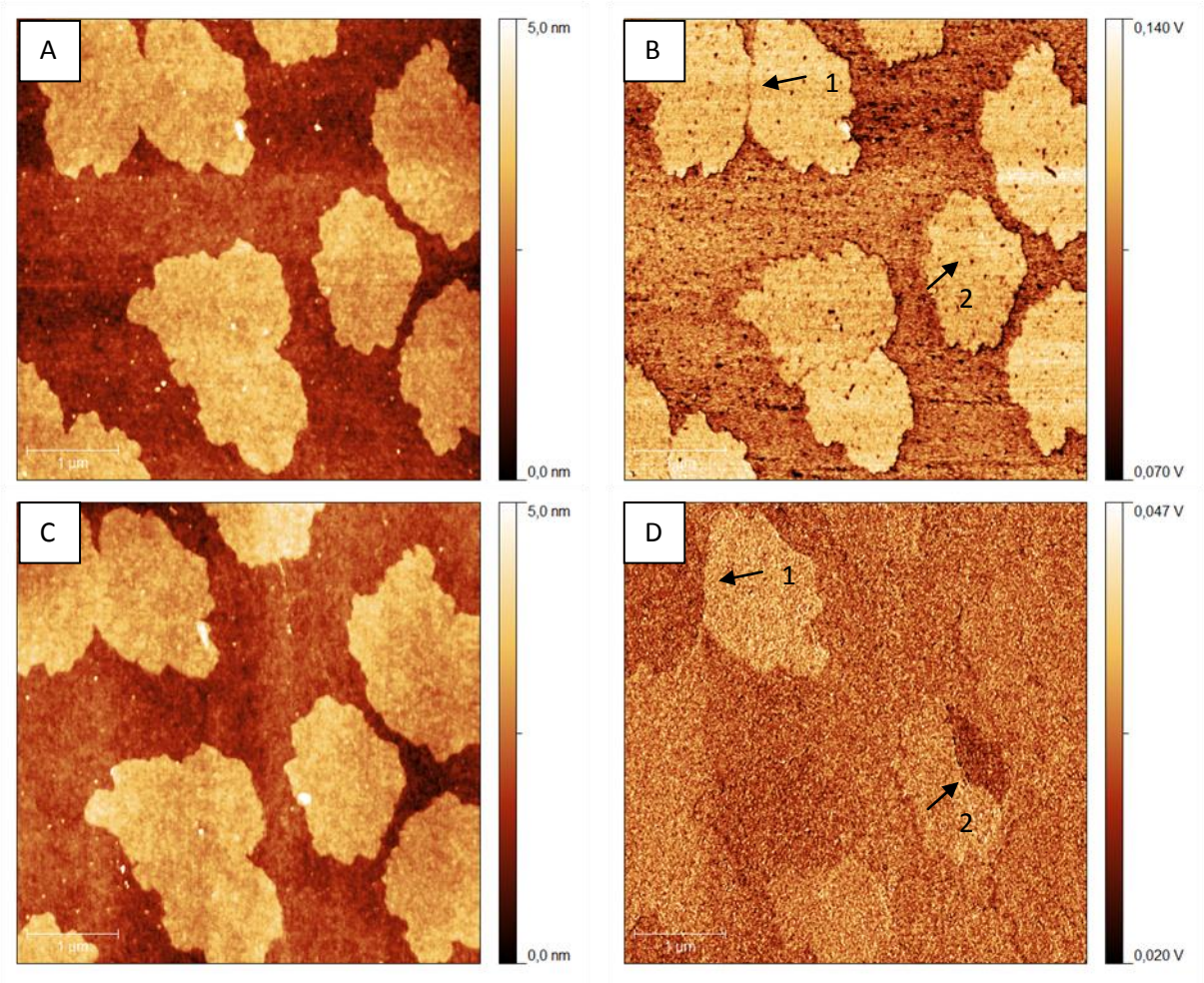

Figure 14: LFM (B) and TSM (D) images of the same area together with the corresponding topography (C and D) images. Arrows 1 and 2 indicate noteworthy features as described in the text. The film was deposited in two steps at a kinetic energy of the impinging molecules of 6.8 eV. *

It could not be due to the coalescence of two grains because then the angle between the crystal orientations would be random. In that case the interface between the grains is smooth and therefore not visible in LFM. Even though this kind of defect is very rarely observed, it is important because it shows that TSM contrast can occur without a corresponding feature in the LFM.

The next set of images is shown in Figure 15. These micrographs refer to a sample grown with SuMBD at rather low kinetic energy, 3.3 eV, and were also collected on the as deposited film. The thickness was such that the first layer is nearly completely coalesced and a significant number of islands had formed on top. Previous research suggests that for the kinetic energy at which this sample was deposited the second layer islands consist of multiple grains.[29] This is evident by TSM contrast within the second layer. Also, as described earlier, LFM contrast within the second layer is a sign of defects such as line dislocations.[25] Considering both LFM and TSM micrographs of the same area should give a more complete picture of the second layer morphology.

Three features are important in Figure 15, which are each indicated with a set of arrows. The first characteristic, indicated by arrows marked with an 1, concerns the contrast in the first layer. Note that the indicated feature is not the only one of this kind in the images. It is, however, a very good example of this kind of detail. In the LFM images, some crack-like lines appear. At the site of these cracks, a significant TSM contrast is visible. This behaviour is identical to the characteristic marked with arrow 1 in Figure 14. The grain structure is very well distinguishable in the first layer, as both the grain boundaries and the different crystal orientations can be identified. There is virtually no contrast difference related to the friction inside these grains.

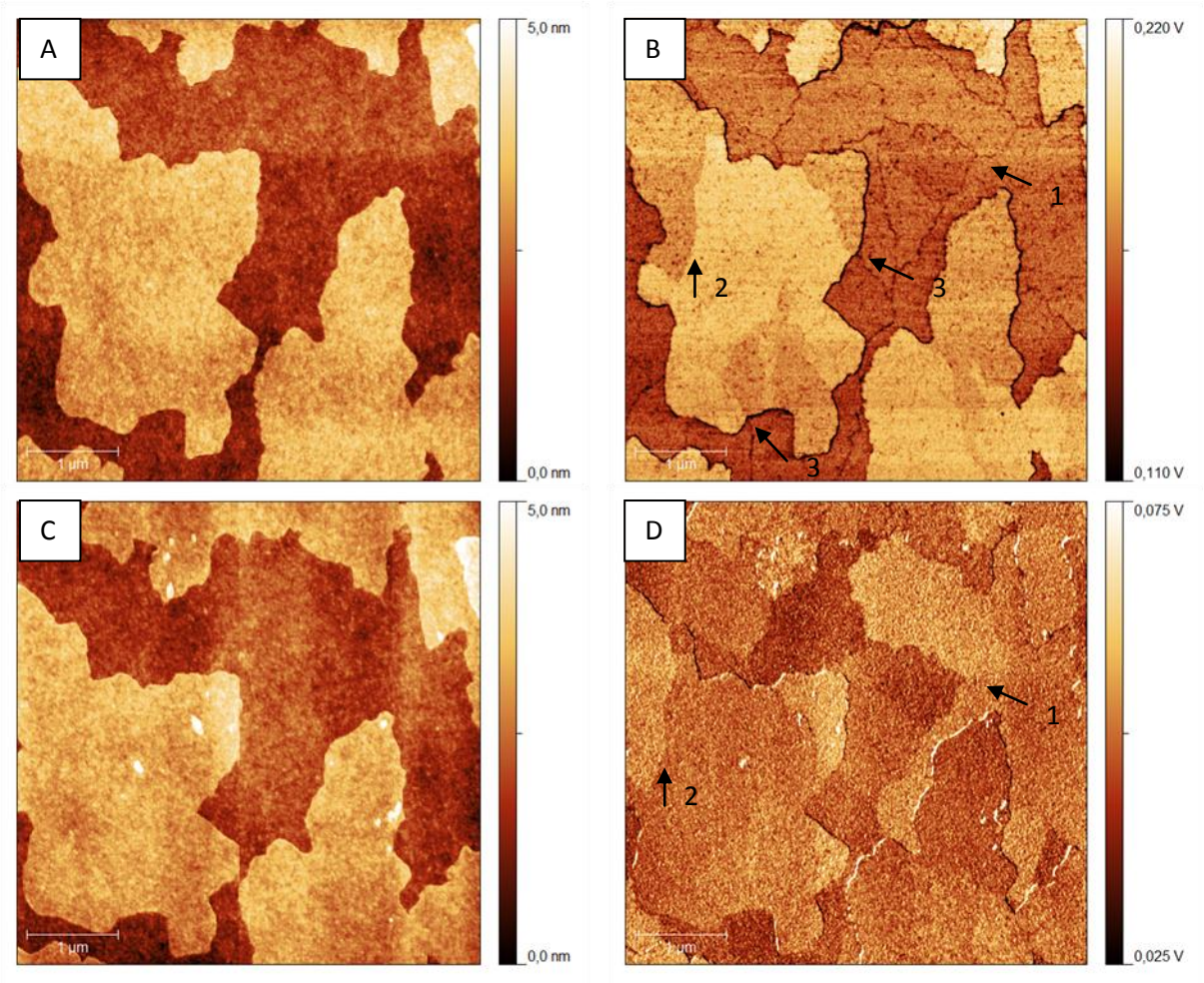

Figure 15: LFM (B) and TSM (D) images of the same area together with the corresponding topography (A and C) images. Arrows 1, 2 and 3 indicate noteworthy features as described in the text. The film was deposited at a kinetic energy of the impinging molecules of 3.3 eV and the coverage is about 1.7 ML. *

The second set of arrows marked with a 2 relate to the contrast in the second layer islands. The same contrast is present in both the LFM and TSM micrographs, albeit with different sign. Note that, again, similar features appear elsewhere on the images. The fact that there is a contrast in the LFM micrograph, but no crack-like lines, indicates that these are not simply different grains which have coalesced. On the contrary, the apparent correlation between LFM and TSM contrast is very surprising. The contrast visible in these micrographs is due to very different types of friction.[16, 17] Also, there seems to be a connection between first layer grain boundaries and the contrast differences in the second layer. This can be clearly seen at the points indicated with the last pair of arrows, marked with a 3. A second layer island covering a grain boundary in the first layer seems to correlate with the occurrence of contrast in the second ML in both LFM and TSM.

The next two series of AFM micrographs, shown in Figure 16 and Figure 17, are both from the same area. Figure 17 shows a detail of Figure 16. The difference between this sample and the previous one is the kinetic energy of the impinging molecules during growth, which was 6.8 eV in this case. The sample thickness is more or less the same as for the sample in Figure 15. Since this sample was deposited using higher energy SuMBD, it should have fewer grain boundaries. However, it is not known whether the defects occurring in this sample are different or similar compared to those present in a low energy SuMBD or OMBD sample. Also the second layer islands should be single crystalline.[29] On examining these AFM images, it becomes clear that the same kinds of contrast peculiarities outlined for Figure 15 are present here. In the large area LFM scan, Figure 16 B,

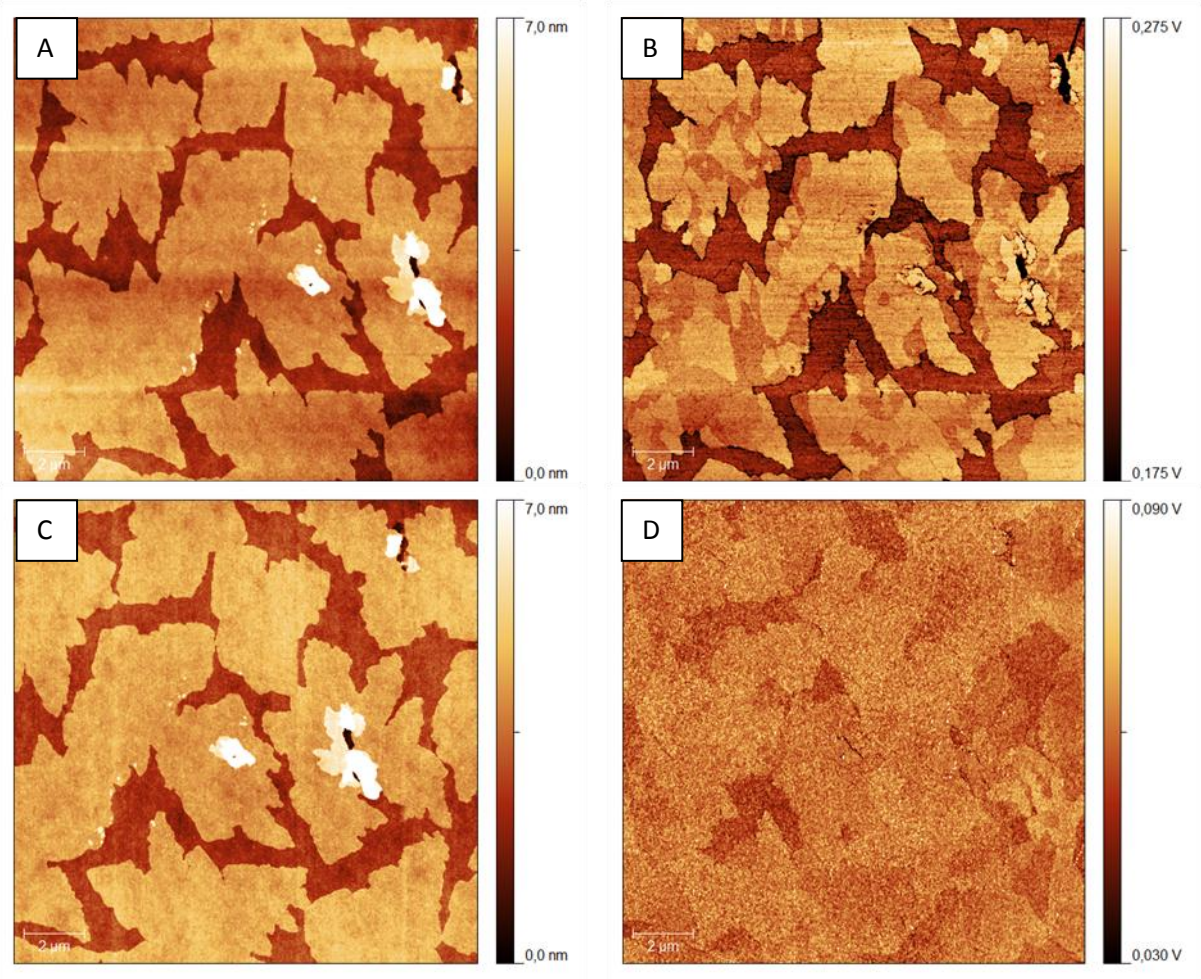

Figure 16: LFM (B) and TSM (D) images of the same area together with the corresponding topography (A and C) images. The film was deposited at a kinetic energy of the impinging molecules of 6.8 eV and the coverage is about 1.5 ML. *

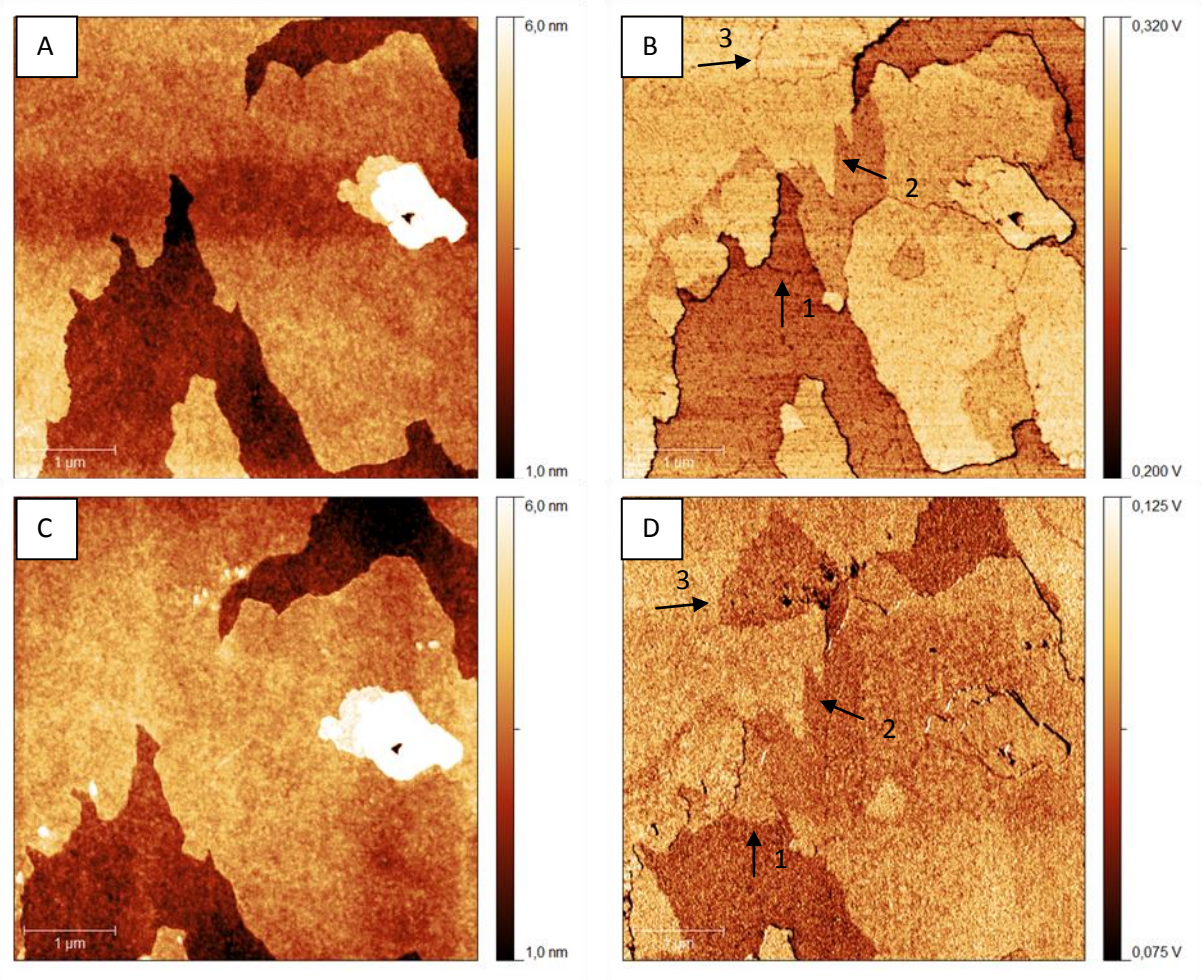

Figure 17: LFM (B) and TSM (D) images of the same area together with the corresponding topography (A and C) images. Arrows 1, 2 and 3 indicate noteworthy features as described in the text. The film was deposited at a kinetic energy of the impinging molecules of 6.8 eV and the coverage is about 1.5 ML. *

the contrast differences in the second layer are striking. Also, several cracks are clearly visible in the first layer. Unfortunately, the contrast in the TSM signal of the same area is not very high. There is virtually no contrast in the second layer. However, it is possible to identify contrast differences in the first layer.

The details become better visible in the second set of images of this sample, shown in Figure 17. Examples of contrast differences in the first and second layers as observed in the previous sample are marked with arrows 1 and 2 again for convenience. The observation of different grains in the first layer of this sample is not surprising, however, the fact that the second layer features are also present is. As stated earlier, second layer islands of films grown at high kinetic energy are expected to be single crystalline and larger than those in a sample grown at lower kinetic energy. Therefore, neither LFM nor TSM contrast was expected within the islands. A third important observation is indicated by arrow 3. Here, a crack-like line is visible in the LFM signal of the second layer. There is no LFM contrast difference observed between the areas on either side of this line. In the TSM, the same feature is visible because of a significant change in contrast. This means that this is an actual grain boundary in the second layer. Unlike the other features observed in the second layer, the behaviour of this is identical to the feature in Figure 14.

To put the above results into context, it is also useful to discuss OMBD grown layers of pentacene. To this end, a single set of AFM images is shown in Figure 18. Three features are marked with arrows 1 to 3. These are examples of the same three important observations found in Figure 17.

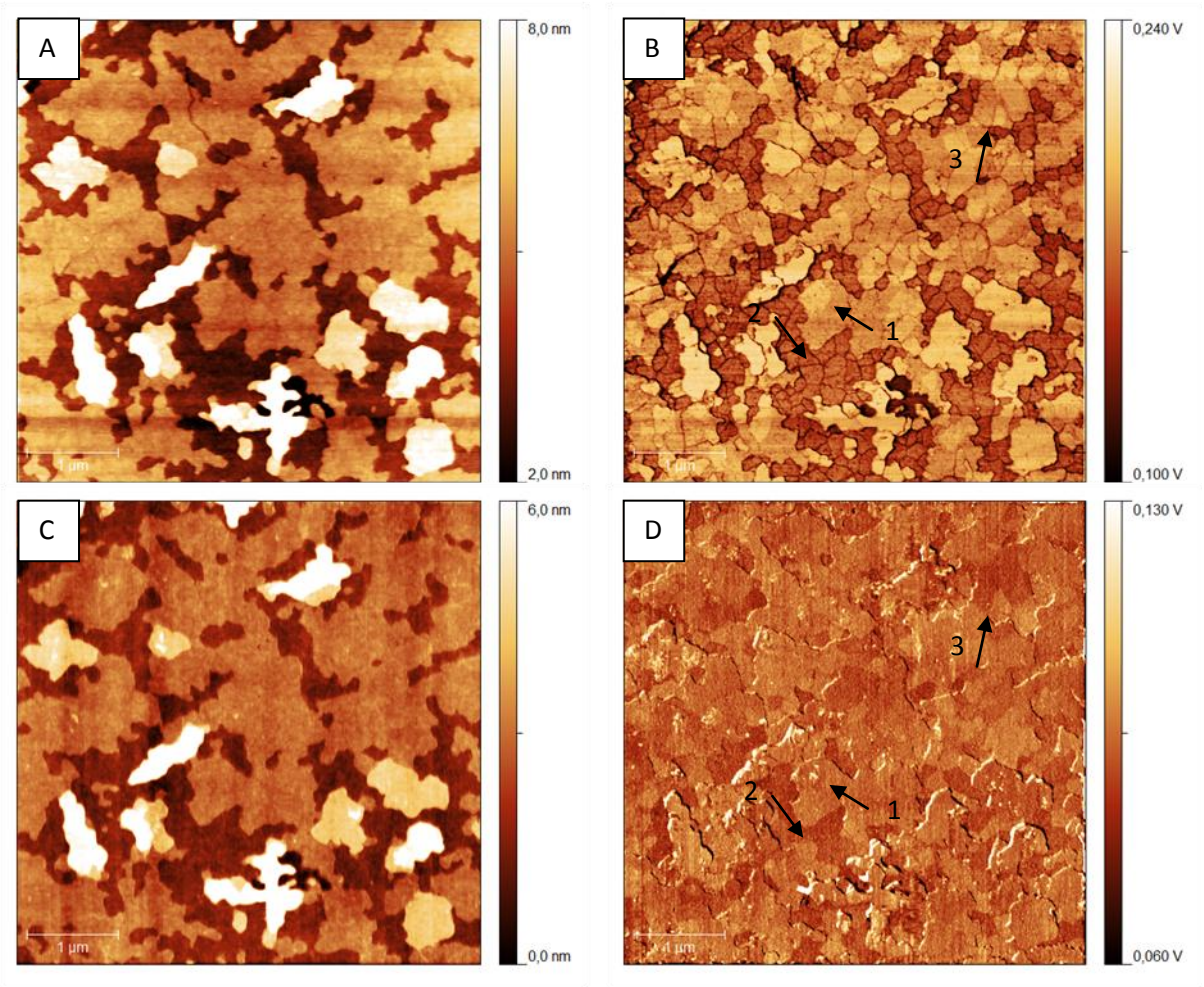

Figure 18: LFM (B) and TSM (D) images of the same area together with the corresponding topography (A and C) images. Arrows 1, 2 and 3 indicate noteworthy features as described in the text. The film was deposited using OMBD.

The only observation that cannot be verified in these films is whether or not there is a correlation between grain boundaries in the first layer and contrast in the second layer, as found in Figure 15. Based on these images, there is no reason to assume that the defect structures in these films are principally different from those grown by SuMBD. When comparing the images in Figure 18 and those in Figure 16, whose real dimensions are only about 1.5 times larger, distinct differences can be observed. First of all, there are many more crack-like lines in the LFM images of the OMBD samples, meaning that the average domain size is significantly smaller in these samples. Also, the second layer islands in the SuMBD samples are predominantly a single crystalline domain, whereas those in the OMBD samples are clearly polycrystalline. Both observations are expected since it is already well established that high energy SuMBD grown layers feature larger domain sizes.

On the other hand, the LFM contrast in the second layer of SuMBD grown films seems to be quite abundant, even when compared to OMBD grown films. This indicates that the dislocations induced by strain in the second layer are also quite common. While this seems surprising, it can easily be explained. The grain sizes in the first and second layer may be significantly larger is SuMBD grown films, the amount of second layer islands growing over a grain boundary is not necessarily so. If the island grows over a grain boundary in the layer below, it will have an epitaxial mismatch resulting in strain and dislocations. Apparently, the large second layer islands in, for example, Figure 16 cover many grain boundaries and therefore contain many strained and defected areas.

The observation of seemingly correlated contrast in the LFM and TSM micrographs is very intriguing and deserves further discussion. Due to the absence of crack-like lines in the LFM images for this particular characteristic suggests the contrast is not due to different crystalline grains.

Another possibility is that symmetric twin boundaries, such as the one found in Figure 14, are very prevalent in the second layer for some reason. However, this seems unlikely and besides the feature in Figure 14 is not accompanied by a contrast in the LFM. Because the correlated contrast does not correspond to a known characteristic, a different explanation should be sought. Assuming that the TSM contrast corresponds to a difference in crystalline orientation and that the LFM contrast corresponds to a difference in the number of defects, the most straightforward explanation would be that a change in crystalline orientation is accompanied by the formation of dislocation lines. This change could be induced by the presence of grains with different orientations in the first layer. This explains the apparent correlation with the grain boundaries in the first layer as well. However, this scenario seems unlikely for a few reasons. First of all, it was previously shown that a change in crystalline orientation does not occur.[6] Instead, part of the second layer island grows in a non-epitaxial way on the first layer. The stress induced by this non-epitaxial growth is the most likely reason the line dislocations are formed.[25] If a change in crystalline orientation occurred, there would be no stress build up and thus no reason to form line dislocation.

Another possibility is that the TSM contrast is influenced by these same dislocations that are responsible for the LFM contrast. In other words, TSM is not only sensitive to the crystalline orientation of the grain, but also to other surface features such as the line dislocations in this sample. There is no difference in the crystalline orientation of the various parts of the second layer even though TSM contrast is present. This is consistent with the fact that the line dislocations are formed to relieve stress which was build up due to non-epitaxial growth. If this is indeed the case, and the TSM signal can be influence by the presence of dislocations or even other defects, this could have a significant impact on the technique of TSM itself. Unfortunately, interpretation of TSM would be less straightforward as care should be taken that the signal is indeed due to differences in the orientation of the grains. On the other side, combining LFM, TSM and possibly other modes can yield an even more detailed picture of the film morphology.

The apparent sensitivity of TSM to the dislocations can be made plausible by considering the structure of these defects as shown in Figure 8. Based on this image, the defects are estimated to occur every few hundred nanometres, which is not very frequent compared to the lattice size. However, they all run parallel to one another and the surface corrugation is significantly larger than the corrugation of a defect free film. In terms of the rigid textures surface model[27], the series defects could be seen as large barriers with an uniform orientation which twist the tip in one particular direction. This is exactly the same as the effect of intrinsic surface corrugation, only on a different scale. The lower frequency of occurrence and the higher impact per corrugation effectively partially cancel each other. Therefore, a significant but sizable effect of these defects on the TSM signal is not unreasonable. One argument against this theory, is that the dislocation lines themselves should be visible in TSM and not a more general effect on the TSM contrast. However, the resolution on the current TSM images might prevent this. The averaging out of the signal is also observed for the TSM signal coming from the regular crystalline anisotropy, but can be resolved when looking at the nanoscopic level.

Even though the contact mode AFM observations were quite unexpected, the following observations were significantly more so. These observations regard contrast differences in the phase maps. Usually, these phase maps contain very little information about the pentacene thin films. In fact, there is no previous report of such a contrast in literature that we are aware of. In this case, two sets of images will be presented. One set contains micrographs of two samples with thicknesses similar to those in the previous figures. The other set contains micrographs of a sample with significantly higher thickness, about 2.5 ML, where the second layer is almost completely coalesced.

The first set of images, seen in Figure 19, is from two different samples. Micrographs A and B are from the same sample as the images in Figure 16 and Figure 17, that is, from a sample deposited at a kinetic energy of 6.8 eV. Micrographs C and D are from a sample deposited at 3.3 eV. In both phase maps clear contrast in the second layer can be observed. Two clear examples are indicated by arrows marked with an 1 in both phase maps. The origin of this phase contrast is completely unclear.

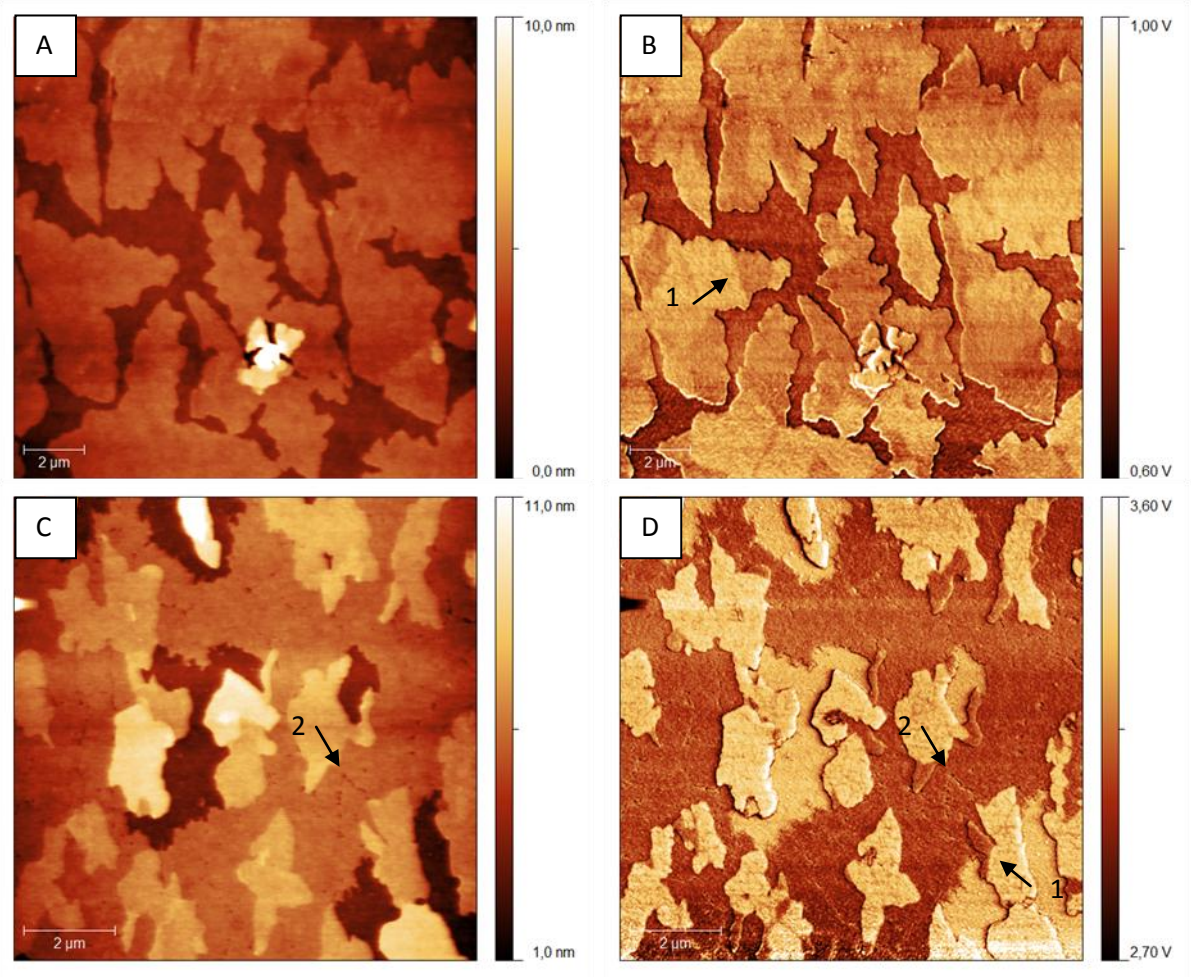

Figure 19: Phase maps (B and D) obtained in tapping mode of two different samples together with the corresponding topography (A and C) images. Arrows 1 and 2 indicate noteworthy features as described in the text. The first film was deposited at a kinetic energy of the impinging molecules of 6.8 eV and the coverage is about 1.5 ML. For the second film the values were 3.3 eV and 1.3 ML. *

Usually, the phase contrast can be attributed to the presence of chemically different adsorbates. It would therefore be tempting to attribute it to water on the sample, but the distribution of this water would be very uncommon. On the other hand, this second layer contrast appears to be very similar to that observed in the LFM images discussed above. This suggests that the origin might be the same. In other words, a difference in defect density could account for the difference in the phase. Also, at the arrow marked with a 2, there seems to be a crack in both the topography and the phase images. This is most likely due to two islands which coalesced along this line and defects have not properly healed. This seems to have occurred between more islands in this particular image.

The next set of images, seen in Figure 20, is from a thicker layer grown at 3.3 eV. The contrast in the phase is very well resolved. The phase contrast occurs mainly in the second layer, which is almost complete, but also in higher layers. A case of phase contrast in the third layer is indicated with arrow 1. Also note that it seems to be somewhat following the contrast in the layer below. What seems to be even more interesting is the fact that the features in topography images correlate somewhat with the features in the phase image, beyond the normal island edges. An example of this is indicated by arrow 2. Again, the reason this contrast in the phase exists it completely unclear.

All in all, it is obvious that there are some interesting features to be found in the LFM, TSM and phase maps of pentacene thin films. These features are not completely understood. Therefore further research is required. First of all, the etching experiments should be conducted once more in order to verify that the line dislocations are indeed present in the second layer of pentacene thin films.

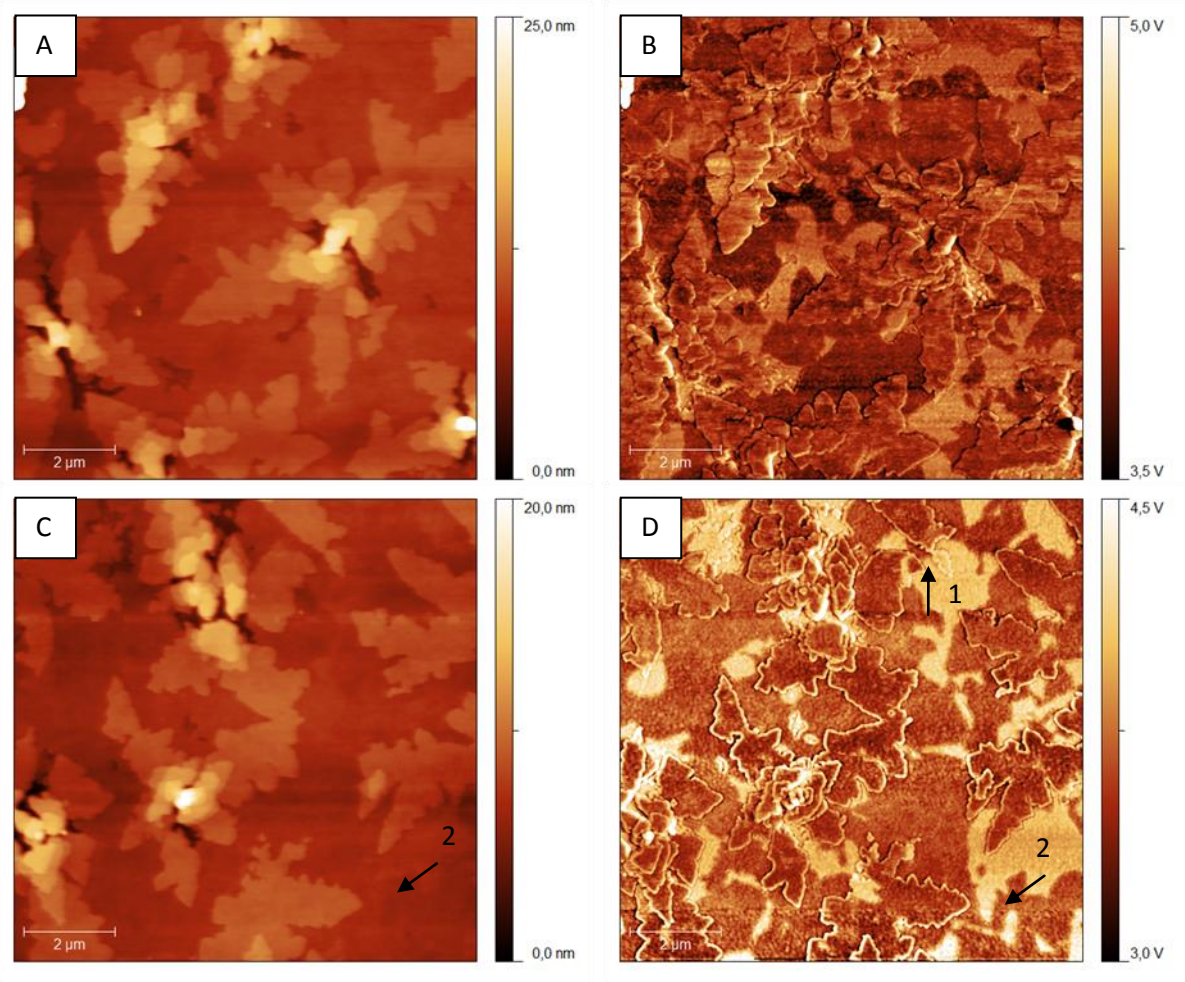

Figure 20: Phase maps (B and D) obtained in tapping mode of two different areas of the same sample together with the corresponding topography (A and C) images. Arrows 1 and 2 indicate noteworthy features as described in the text. The film was deposited at a kinetic energy of the impinging molecules of 3.3 eV and the coverage is about 2.5 ML. *

If these are indeed present in the regions with both LFM and TSM contrast, the hypothesis that the TSM signal can be influenced by defect structures in the film can be strengthened. Possibly AFM in UHV could be used to obtain higher quality LFM and TSM images. Theoretical work on the relation between TSM contrast and possible defects would also be useful. The origin of the contrast in the phase maps also deserves further investigation. In this case, UHV AFM would be useful as well, to exclude the possibility that a water layer is imaged.

Miscellaneous samples

Besides the main set of experiments involving the defect structures of the pentacene thin layers, several other experiments have been conducted as well. First off all, two interesting samples were made in collaboration with Stefano Gottardi, who worked extensively on the same SuMBD setup last year. These samples were grown to gain more insight into the principle growth dynamics of SuMBD. More specifically, these experiments were designed to get a better understanding of the influence of a native water layer on the sample on the nucleation and growth of the pentacene films. To this end, a liquid nitrogen cooled water trap was inserted in the helium line to freeze out the water. This way, the possible effect of water deposited from the beam is eliminated. Of course, this precaution does not prevent the formation of a water layer due to water still present in the residual gas atmosphere in the chamber.

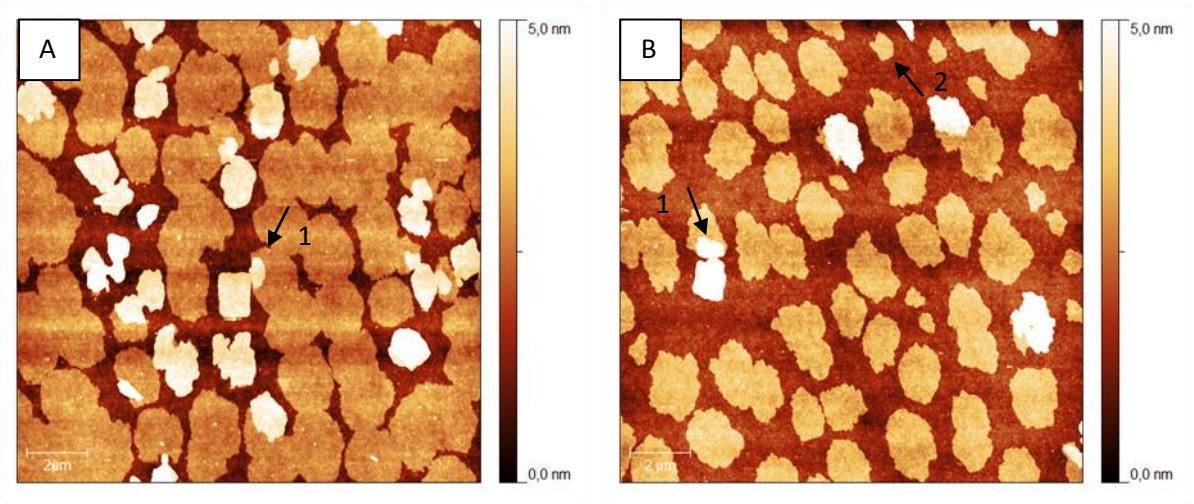

Figure 21: Topography images of two samples grown in two stages. The first film was deposited at a kinetic energy of the impinging molecules of 6.8 eV followed by 3.3 eV (A). For the second film the values were 6.8 eV for both steps (B).

These samples were grown in two stages. The first stage was a 12 min deposition at 6.8 eV. The second stage was a 6 min deposition at either 6.8 or 3.3 eV. The second growth step was performed after about 5 hours, while the samples were kept in vacuum. However, the rate was very unstable during the deposition, apparently due to the LN_2 trap. While depositing, the liquid nitrogen would evaporate, which somehow changed the pressure in and/or the flux trough the gas line, and hence the deposition rate. The pressure fluctuation was not such that the kinetic energy of the pentacene molecules was altered significantly. Due to instable rate, the thicknesses of the samples are quite different, so the two samples are hard to compare. This limits the amount of useful information that can be extracted from them.

Topography images of the samples are shown in Figure 21. In the high energy low energy sample, shown in Figure 21 A, the first ML started to coalesce and a second ML island has formed on multiple sites. However, the second island growth is unusual. Instead of small islands on top of excising islands, entire grains are two layers thick. Moreover, at points where two grains start to coalesce the second layer is flowing onto the neighbouring grain. This can be seen at arrow 1. This unusual behaviour is a clear indication that a water layer was formed on the sample during the 5 hours between deposition and this water layer has a profound effect on the deposition. Getting rid of this water layer could therefore be a good method to improve thin film formation. In the high energy high energy sample, shown in Figure 21 B, the same effect can be observed, again marked with arrow 1. Also, due to the fact that the first layer is not as completed as in the other sample, another effect can be observed. This is indicated with arrow 2. This and other islands are significantly smaller than the average. This shows that they are nucleated at a later stage than the large islands. Most likely, this nucleation occurred during the second growth step. This shows that the possible water layer formed makes the two growth steps behave as if they were independent. Nucleation of new islands seems to be favoured over growth of the existing islands. Since the pentacene molecules deposited at high energy could more readily overcome any barriers due to the water layer, it is expected that high energy growth would yield less new nucleation and more growth of existing islands. However, due to the instable rates, the amount of second layer nucleation could not be compared and this expectation could not be verified.

Also, a collaboration was established with Dr. V. K. Thorsmølle and co-workers. This work required the growth of a thick film of pentacene on a single crystal of MgO by SuMBD. This sample will be used to do ultrafast optical measurements on the dynamics of excited states. In short, the excited state in pentacene crystals, created by photoexcitation, evolves rapidly into a dark state.

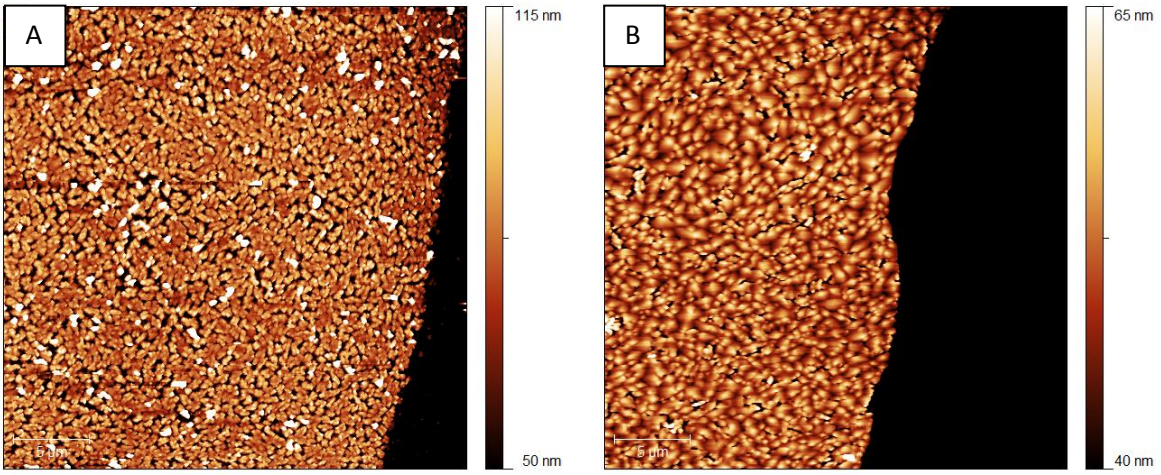

Figure 22: Topography images of thick pentacene films grown on MgO (A) and SiO_x (B). The black area is bare substrate, which was not exposed to the pentacene due to the presence of a mask.

This occurs via singlet-to-triplet fission. This is very a favourable process because it enables multiple exciton formation and the harvesting of high energy photons. This is particularly useful in photovoltaic devices. However, it was found that this fission process is suppressed in thin films, which were grown using OMBD. This is most likely due to the many defects in these films. SuMBD grown films usually have a much lower defect density compared to the OMBD grown films. Therefore, a higher fission rate would be expected for the SuMBD grown films.

The results of the measurements conducted by the co-workers of Dr. Thorsmølle are not yet available. However, AFM images were taken of one of the two thick films of pentacene on MgO single crystals as well as a pentacene film on SiO_x grown alongside it. The images were taken at a part of the sample which was partially covered with a mask. This was done to enable the possibility of determining the step height, and thus the film thickness. These AFM images are shown in Figure 22. The area is the same size in both cases. The bare film that was under the mask is black to optimize the contrast within the films. The important thing here is the difference in the films. The films deposited on MgO seem to be composed of significantly smaller grains. Also, the film seems to be less dense because of this. Moreover, the thickness of the film grown on MgO is lower. It is about 15 nm while the pentacene film on SiO_x is over 25 nm thick. This is the case even though the SiO_x sample was positioned more to the side of the beam. Based on these few observations, it is reasonable to conclude that pentacene grows better on SiO_x than on MgO. This is somewhat surprising considering the fact that the former substrate is amorphous and the latter is single crystalline. At least, a better quality film should be expected. The difference in thickness can very well be explained by a difference in sticking factor.

Conclusion and outlook

In this work, the defect structures of pentacene thin films have been investigated. More precisely, the aim was to show whether or not certain dislocation lines were present in the second monolayer of SuMBD grown pentacene thin films. These dislocations were previously reported in literature for pentacene thin films grown using the conventional technique of OMBD. These defects can be visualised by a short etching step in diluted sulphuric acid. Therefore, this etching procedure would have been ideally suited for this research. However, there were some key steps to this etching procedure that were not mentioned in literature. Consequently, not a single dislocation line was observed in any of the samples deposited in this work. This included several OMBD grown films. However, a significant amount of indirect evidence for defects was present in the many AFM images recorded. The presence of specific contrasts in LFM and TSM images on the same area invite the conclusion that dislocations should be present in the SuMBD grown films as well. However, more research is required to obtain hard evidence for this conclusion.

A second conclusion that can be made based on the aforementioned contrast in the LFM and TSM signals is that there is significant evidence suggesting that TSM is not only sensitive to the orientation of the pentacene crystals. In this case, correlations between the LFM and TSM contrast indicates that some of the contrast is due to the dislocation lines which are most likely present in the second layer of the film. Some similar contrast has been observed in several phase maps, obtained in tapping mode, as well. The reason why this is possible is not clear at this point. Both points raised here warrant further investigation to obtain more solid evidence.

Bibliography

[1] A.K. Bakhshi and G. Bhalla, J. Sci. Ind. Res. **63**, 715-728 (2004)
[2] H. Dong, C. Wang and W. Hu, Chem. Commun. **46**, 5211-5222 (2010)
[3] R.B. Campbell, J.M. Robertson and J. Trotter, Acta Cryst. **14**, 705-711 (1961)
[4] S.E. Fritz, S.M. Martin, *et. al.*, J. Am. Chem. Soc. **126**, 4084-4085 (2004)
[5] C.D. Dimitrakopoulos, A.R. Brown and A. Pomp, J. Appl. Phys. **80**, 2501-2508 (1996)
[6] V. Kalihari, D.J. Ellison, *et. al.*, Adv. Mater. **21**, 3092-3098 (2009)
[7] G. Horowitz, Adv. Mater. **10**, 365-377 (1998)
[8] G. Horowitz, X.Z. Peng, *et. al.* Synth. Met. **51**, 419-424 (1992)
[9] S.F. Nelson, Y.Y. Lin, *et. al.*, IEEE Electron. Device Lett. **18**, 606-608 (1997)
[10] K.C. Liao, A.G. Ismail, *et. al.*, Adv. Mater. **22**, 3081-3085 (2010)
[11] H. Klauk, M. Halik *et. al.*, J. Appl. Phys. **92**, 5259-5263 (2002)
[12] S. Lee, B. Koo *et. al.*, Appl. Phys. Lett. **88**, 162109-& (2006)
[13] T. Toccoli, A. Pallaoro *et. al.*, Appl. Phys. Lett. **88**, 132106-& (2006)
[14] S. Pratontep, M. Brinkmann *et. al.*, Phys. Rev. B **69**, 165201-& (2004)
[15] J.G. Amar, F. Family and P.M. Lam, Phys. Rev. B **50**, 8781-8797 (1994)
[16] A.C. Mayer, R. Ruiz *et. al.*, Phys. Rev. B **73**, 205307-& (2006)
[17] S. Iannotta and T. Toccoli, J. Polym. Sci. Pol. Phys. **41**, 2501-2521 (2003)
[18] R. Campargue, J. Phys. Chem. **88**, 4466-4474 (1984)
[19] A. Kantrowitz and J. Grey, Rev. Sci. Instrum. **22**, 328-332 (1951)
[20] D.R. Millar: in Atomic and Molecular Beam Methods, G. Scoles (ed.), Oxford University Press, Oxford (1955)
[21] V.H. Reist and J.B. Fenn, J. Chem. Phys. **39**, 3240-3250 (1963)
[22] V. Aquilanti, D. Ascenzi *et. al.*, J. Chem. Phys. **99**, 13620-13626 (1995)
[23] J.A. Last and M.D. Ward, Adv. Mater. **8**, 730-733 (1996)
[24] V. Kalihari, E.B. Tadmor, *et. al.*, Adv. Mater. **20**, 4033-4039 (2008)
[25] K. Puntambekar, J. Dong *et. al.*, Adv. Funct. Mater. **16**, 879-884 (2006)
[26] V. Kalihari, G. Haugstad and C.D. Frisbie, Phys. Rev. Lett. **104**, 086102-& (2010)
[27] M. Campione and E. Fumagalli, Phys. Rev. Lett. **105**, 166103-& (2010)
[28] T. Toccoli, Organic Thin Film Growth by Supersonic Molecular Beams for Device Applications, Zernike Institute for Advanced Materials, Groningen, Ph.D. Thesis (2007)
[29] Y. Wu, T. Toccoli *et. al.*, Appl. Phys. A **95**, 21-27 (2009)